Kinetic theory of surface plasmon polariton in semiconductor nanowires

Y. Yin* and M. W. Wu†

Hefei National Laboratory for Physical Sciences at Microscale and Department of Physics, University of Science and Technology of China, Hefei, Anhui 230026, China

(Received 21 November 2012; revised manuscript received 16 January 2013; published 8 April 2013)

Based on the semiclassical model Hamiltonian of the surface plasmon polariton and the nonequilibrium Green-function approach, we present a microscopic kinetic theory to study the influence of the electron scattering on the dynamics of the surface plasmon polariton in semiconductor nanowires. The damping of the surface plasmon polariton originates from the resonant absorption by the electrons (Landau damping), and the corresponding damping exhibits size-dependent oscillations and distinct temperature dependence without any scattering. The scattering influences the damping by introducing a broadening and a shifting to the resonance. To demonstrate this, we investigate the damping of the surface plasmon polariton in InAs nanowires in the presence of the electron-impurity, electron-phonon, and electron-electron Coulomb scatterings. The main effect of the electron-impurity and electron-phonon scatterings is to introduce a broadening, whereas the electron-electron Coulomb scattering can not only cause a broadening, but also introduce a shifting to the resonance. For InAs nanowires under investigation, the broadening due to the electron-phonon scattering dominates. As a result, the scattering has a pronounced influence on the damping of the surface plasmon polariton: the size-dependent oscillations are smeared out and the temperature dependence is also suppressed in the presence of the scattering. These results demonstrate the important role of the scattering on the surface plasmon polariton damping in semiconductor nanowires.

DOI: 10.1103/PhysRevB.87.165412 PACS number(s): 73.20.Mf, 73.22.Lp, 72.30.+q, 71.10.−w

I. INTRODUCTION

Since the pioneering theoretical work by Ritchie[1] and the electron-loss spectroscopy measurements by Powell and Swan,[2] the physics of surface plasmon polariton (SPP) has been extensively studied for more than five decades.[3–9] SPPs are electromagnetic (EM) waves coupled to the collective excitations of electrons on the surface of a conductor.[10,11] In this coupling, the electrons oscillate collectively in resonance with the EM waves and hence trap the EM waves on the surface. The resonant coupling leads to the SPPs and gives rise to their unique properties, such as the enhancement of the surface electric fields and the slowing down of the group velocity of the EM waves.[12–20] Applications exploiting these properties have been widely studied in biosensing,[21] solar cells,[22] quantum information processing,[23–25] subwavelength optical imaging, and waveguiding devices.[11,26–31]

The SPPs often suffer from dissipative losses.[32] Overcoming the losses is crucial for the improvement of performance of many SPP-based devices, such as the fidelity of the waveguide and the sensitivity of the single-molecule sensor.[21,33] An effective modulation of the losses is also highly desirable for the active plasmonic devices proposed in recent years.[34–36] Thus a thorough understanding of the damping processes responsible for the dissipative losses is essential. Since the SPPs in metals have been the major focus for many decades, previous studies on the damping processes have traditionally been focused on metals. It is found that the dominant damping process is the decay of the SPPs into electrons, i.e., the Landau damping.[37–41] The interband transitions and the many-body exchange-correlations can have pronounced influences on the Landau damping. These influences can be incorporated into microscopic models based on time-dependent density-functional theory or a semiclassical model Hamiltonian of the SPP.[42–44] Calculations based on these models have shown good agreement with experiments.[45–47]

In recent years, doped semiconductors, such as SiC, GaAs, InAs, Cu_2S, and Cu_2Se are suggested as promising candidates to replace metals in SPP applications.[48–52] The SPPs in doped semiconductors are characterized by their substantial low losses and tunable frequencies.[53–56] They are also easier to be manipulated via doping or external electric/magnetic fields and to be integrated into complex, functional circuits.[57–59] The further development of the SPPs in doped semiconductors requires a better understanding of their damping processes. However, the physics involved in doped semiconductors can be quite different from that in metals. For doped semiconductors, although the Landau damping is still believed to be the leading damping process at large wave vectors,[60,61] the charge depletion/accumulation layer[62,63] and the electron scattering[64,65] are found to have important influence on the damping. Of particular importance is the effect of the electron scattering, since the typical scattering rate can be comparable to the SPP frequency in semiconductors. However, to the best of our knowledge, this effect has only been discussed by using phenomenological relaxation times.[64,65] A microscopic theory exploiting this effect has not been established yet.

In this paper, by combining the semiclassical model Hamiltonian of the SPP[42–45] and the nonequilibrium Green-function approach,[66,67] we present a microscopic kinetic theory to study the damping of the SPP in doped semiconductors, within which the relevant electron scatterings are treated fully microscopically. The main purpose of this work is to understand the influence of these scatterings on the Landau damping of the SPP. To demonstrate this, we focus here on the SPPs in InAs nanowires[23,28,29,51] and concentrate on the electron-impurity (ei), electron-phonon (ep), and electron-electron (ee) Coulomb scatterings. We find that the scattering can have pronounced

influences on the Landau damping of the SPP by modulating the resonance between the electrons and the SPPs. Different scattering has different effect on the resonance. The main effect of the ei and ep scatterings is to introduce a broadening to the resonance, whereas the ee scattering can not only cause a broadening, but also introduce a shifting to the resonance. For InAs nanowires, the ep-scattering–induced broadening is found to be the dominant effect. These effects can lead to a pronounced influence on the damping of the SPP, which can be seen from both the size and temperature dependence of the SPP damping: (1) the size-dependent oscillations of the SPP damping are smeared out and (2) the temperature dependence of the SPP damping is suppressed by the scattering. These results demonstrate the important role of the electron scattering on the SPP damping.

This paper is organized as follows. In Sec. II, we introduce the semiclassical model Hamiltonian of the SPP for semiconductor nanowires and briefly outline the derivation of the kinetic equations. We also present an analytic solution for the SPP damping which provides a simple and physically transparent picture to understand the influence of the scattering on the SPP damping process. In Sec. III, we discuss in detail the influence of the electron scattering on the SPP damping by numerical solving the kinetic equations. The importance of the scattering is demonstrated by studying its influences on the temperature and size dependence of the SPP damping. The analytic solution is also compared with the numerical ones in this section. We summarize and discuss in Sec. IV.

II. MODEL AND FORMALISM

A. Semiclassical model for SPP-electron system

We consider an n-type free-standing cylindrical nanowire with radius R as illustrated in Fig. 1(a). The z axis is chosen to be along the wire. Following the semiclassical approach developed in previous works,[42–45] we decompose the Hamiltonian into

$$H = H_{\rm SPP} + H_{\rm el} + H_{\rm SPP\text{-}el}, \tag{1}$$

where $H_{\rm SPP}$, $H_{\rm el}$, and $H_{\rm SPP\text{-}el}$ are Hamiltonians for the SPP, electrons and the SPP-electron coupling, respectively. Here we only present the Hamiltonian, leaving the details to Appendix A.

For nanowires, there exists one fundamental SPP mode with axial symmetry, which has no cutoff at low frequency and has been found to be important for both the terahertz emission and quantum subwavelength optics.[23,28,29,51] In this paper, we focus on the dynamics of this SPP mode. The corresponding Hamiltonian takes the form

$$H_{\rm SPP} = \sum_q \Omega_q b_q^\dagger b_q, \tag{2}$$

where $b_q(b_q^\dagger)$ represents the annihilation(creation) boson operator for the SPP, with Ω_q being the corresponding dispersive relation illustrated in Fig. 1(b). Note that we set $\hbar = 1$ throughout this paper.

The Hamiltonian of electrons can be written as

$$H_{\rm el} = H_{\rm el}^0 + H_{\rm ei} + H_{\rm ep} + H_{\rm ee}, \tag{3}$$

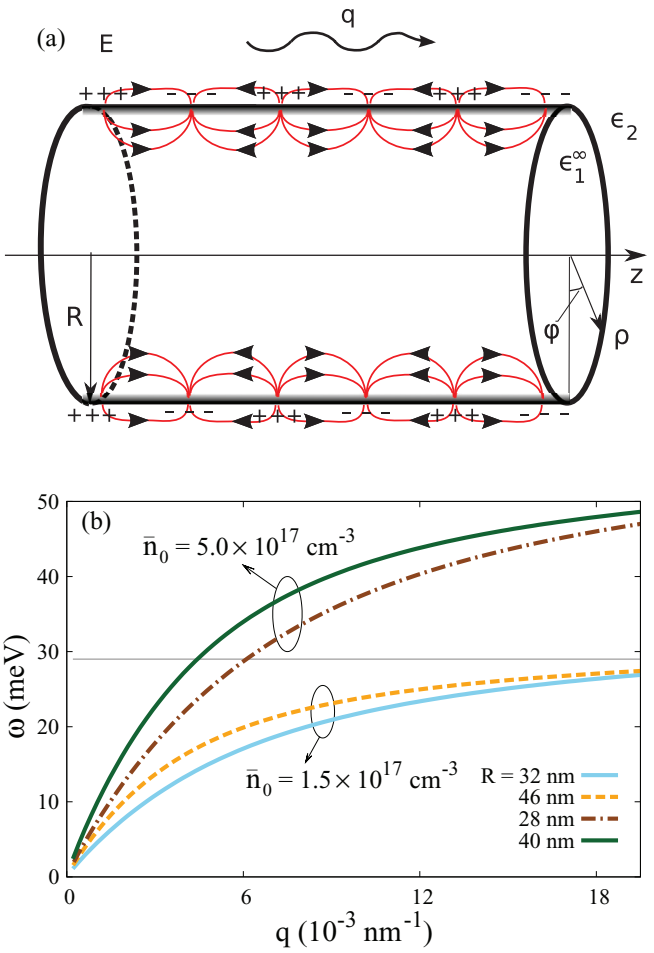

FIG. 1. (Color online) (a) Schematic of the structure of the electron field E and corresponding surface charge of the axial symmetric SPP mode in a cylindrical nanowire. ϵ_1^∞ (ϵ_2) is the dielectric constant inside (outside) the nanowire. The red curves with arrows represent the electric fields of the SPP mode. (b) The dispersive relation of the axial symmetric SPP mode for nanowires with different electron density $\bar{n}_0$ and wire radius R. The thin grey line marks the energy of the LO phonon.

where the free-electron Hamiltonian $H_{\rm el}^0$ is modelled by a mean-field potential. The interaction Hamiltonians $H_{\rm ei}$, $H_{\rm ep}$, and $H_{\rm ee}$ represent the ei, ep, and ee interaction, respectively.

By choosing the mean-field potential to be an infinite cylindrical potential well with radius R, the free-electron Hamiltonian $H_{\rm el}^0$ can be written as

$$H_{\rm el}^0 = \sum_{nk\sigma} \varepsilon_k^n c_{nk\sigma}^\dagger c_{nk\sigma}, \tag{4}$$

in which $\varepsilon_k^n = \frac{k^2 + (\lambda_{\tilde{n}}^{\tilde{m}}/R)^2}{2m^*}$ is the eigenenergy with m^* representing the electron effective mass. The composed index $n = (\tilde{m},\tilde{n})$ labels the electron subband with $\tilde{m}$ and $\tilde{n}$ representing the angular and radial quantum numbers, respectively. $\lambda_{\tilde{n}}^{\tilde{m}}$ denotes the $\tilde{n}$th zero of the Bessel function of the first kind $J_{\tilde{m}}(x)$. The corresponding eigenstates read

$$\psi_{nk}(\rho,\varphi,z) = \frac{J_{\tilde{m}}\left(\lambda_{\tilde{n}}^{\tilde{m}}\rho/R\right)}{\sqrt{\pi R} J_{\tilde{m}+1}\left(\lambda_{\tilde{n}}^{\tilde{m}}\right)} e^{i\tilde{m}\varphi} e^{ikz}. \tag{5}$$

The ei interaction Hamiltonian can be written as

$$H_{\rm ei} = \sum_{i}^{N_i} \sum_{kq\sigma} v_q^{nn'} \rho_i(q) c^{\dagger}_{n'k+q\sigma} c_{nk\sigma}, \tag{6}$$

with N_i being the total impurity number and $\rho_i(q) = e^{-iqz_i}$. Here we have assumed that the impurities are distributed on the surface of the nanowire with an axially symmetric distribution. $v_q^{nn'}$ is the matrix element for the ei interaction. The ep interaction Hamiltonian can be written as

$$H_{\rm ep} = \sum_{\boldsymbol{Q}q} \sum_{nn'k\sigma} M^{nn'}_{\boldsymbol{Q}q} (a_{\boldsymbol{Q}q} + a^{\dagger}_{-\boldsymbol{Q}-q}) c^{\dagger}_{nk\sigma} c_{n'k-q\sigma}, \tag{7}$$

where $a_{\boldsymbol{Q}q}(a^{\dagger}_{\boldsymbol{Q}q})$ represents the annihilation(creation) operator for the LO phonons, with $\boldsymbol{Q}$ and q representing the components of the phonon momentum perpendicular and parallel to the nanowire. Here, we use bulk phonons in the present investigation, which is valid for nanowires with large diameters.[68,69] $M^{nn'}_{\boldsymbol{Q}q}$ is the matrix element for the ep interaction. It is noticed that although surface-optical (SO) phonons[69] also exist in nanowires, they are of marginal importance since the corresponding electron-SO-phonon interaction is rather weak compared with the electron-LO-phonon interaction for the nanowires we consider here. The influence of the SO phonons will be further addressed in Sec. III B. The ee interaction Hamiltonian can be written as

$$H_{\rm ee} = \sum_{kk'q} \sum_{nn'} \sum_{\sigma\sigma'} V_q^{nn'} c^{\dagger}_{nk\sigma} c^{\dagger}_{n'k'\sigma'} c_{n'k'+q\sigma'} c_{nk-q\sigma}, \tag{8}$$

where $V_q^{nn'}$ is the matrix element for the ee interaction. The SPP-electron coupling Hamiltonian $H_{\rm SPP\text{-}el}$ can be written as

$$H_{\rm SPP\text{-}el} = \sum_{nk\sigma} \sum_{n'k'} g^{nn'}_{k-k'} (b_{k-k'} + b^{\dagger}_{k'-k}) c^{\dagger}_{nk\sigma} c_{n'k'\sigma}, \tag{9}$$

where $g_q^{nn'}$ is the SPP-electron coupling matrix element. In these equations, matrix elements $v_q^{nn'}$, $M^{nn'}_{\boldsymbol{Q}q}$, $V_q^{nn'}$ and $g_q^{nn'}$ are given in detail in Appendix A.

B. Kinetic equations

In this section, we briefly outline the derivation of the kinetic equations for the SPP-electron system. The details can be found in Appendix B.

The damping of the SPP is obtained by studying the temporal evolution of a coherent SPP wave packet with central wave vector Q_s, which can be expressed as $|B_s\rangle = \sum_q p_q^{Q_s} e^{-\frac{1}{2}|B_q|^2} e^{b_q b^{\dagger}_q} |0\rangle$ (see Ref. 70). The line-shape function of the wave packet $p_q^{Q_s}$ is chosen to be $p_q^{Q_s} = \frac{\sin[(Q_s-q)L/2]}{(Q_s-q)L/2}$, where L is the wave packet length. Such wave packet is typical in a Fabry-Perot SPP resonator, which has been observed in various SPP systems.[25,71–73]

The amplitude of the wave packet can be described by $B_s = \sum_q p_q^{Q_s} B_q$. The kinetic equation of B_s is obtained from the Heisenberg equation of the SPP annihilation operator b_q, which has the form

$$\partial_t B_s(t) = \sum_{nn',kk',\sigma} p^{Q_s}_{k-k'} g^{nn'}_{k-k'} G^{<}_{\sigma}(n'k',nk;tt), \tag{10}$$

where $G^{<}_{\sigma}(nk,n'k';tt')$ is the "lesser" electron Green function defined as $G^{<}_{\sigma}(nk,n'k';tt') = i\langle c^{\dagger}_{n'k'\sigma}(t') c_{nk\sigma}(t)\rangle$ (see Ref. 66).

The kinetic equation of the electron Green function $G^{<}_{\sigma}(nk,n'k';tt)$ is derived by using the nonequilibrium Green-function approach, which can be written as

$$\begin{aligned}\left[-i\partial_t - \left(\varepsilon^{n'}_{k'} - \varepsilon^{n}_{k}\right)\right] G^{<}_{\sigma}(nk,n'k';tt) \\ = \sum_{\bar{n}q} (B_{-q} + B^{\dagger}_{q}) \left[g^{\bar{n}n'}_{q} G^{<}_{\sigma}(nk,\bar{n}k'-q;tt) \right. \\ \left. - g^{n\bar{n}}_{q} G^{<}_{\sigma}(\bar{n}k+q,n'k';tt)\right] + I^{<\sigma}_{nk,n'k'}(t),\end{aligned} \tag{11}$$

where the first term in the right-hand side of the equations is the coherent driving term of the SPP, while the second term is the scattering term consisting the ei, ep, and ee scatterings.

Within the rotating wave approximation relative to the SPP central frequency Ω_s,[66,67] we obtain the kinetic equations for the SPP-electron system:

$$\partial_t \bar{B}_s(t) = -i \sum_{nn'\sigma} \sum_{kk'} p^{Q_s}_{k-k'} g^{nn'}_{k-k'} [P_{\sigma}(nk,n'k';t)]^{\dagger}, \tag{12}$$

$$\begin{aligned}\partial_t P_{\sigma}(nk,n'k';t) &= i\omega^{nn'}_{kk'} P_{\sigma}(nk,n'k';t) \\ &\quad + i g^{nn'}_{k-k'} p^{Q_s}_{k-k'} \bar{B}^{\dagger}_{s} [f_{n\sigma}(k) - f_{n'\sigma}(k')] \\ &\quad + \bar{I}^{\sigma}_{nk,n'k'},\end{aligned} \tag{13}$$

with the detuning

$$\omega^{nn'}_{kk'} = \varepsilon^{n'}_{k'} - \varepsilon^{n}_{k} - \Omega_s. \tag{14}$$

In the above equations, $\bar{B}_s(t) = B_s(t) e^{i\Omega_s t}$ and $P_{\sigma}(nk,n'k';t) = -iG^{<}_{\sigma}(nk,n'k';tt) e^{i\Omega_s t}$ represent the SPP amplitude and electron polarization, respectively. $f_{n\sigma}(k)$ represents the equilibrium electron distribution which is conventionally chosen to be the spin-unpolarized Fermi-Dirac distribution at temperature T.

It should be emphasized that in the derivation, we have treated the SPP-electron coupling $g_q^{nn'}$ perturbatively and linearized the equations by keeping only terms up to the linear order of $g_q^{nn'}$. Thus the SPP couples only to the electron polarization corresponding to the off-diagonal electron Green function with respect to the electron momentum k and subband index n.

The scattering term within the rotating wave approximation can be expressed as $\bar{I} = \bar{I}^{\rm ei} + \bar{I}^{\rm ep} + \bar{I}^{\rm ee}$, where $\bar{I}^{\rm ei}$, $\bar{I}^{\rm ep}$, and $\bar{I}^{\rm ee}$ are contributions from the ei, ep, and ee scatterings, respectively. Their expressions can be found in Appendix B.

C. Landau damping process

In the kinetic equation (13) describes the resonant excitation of the electron polarizations, while Eq. (12) describes the back-action of the polarizations to the SPP. The summation in Eq. (12) implies that even without any scattering, the phase-mixing between polarizations with different frequencies can also lead to the damping of the SPP, which is the origin of the Landau damping.

To further clarify the Landau damping process described by the kinetic equations, we solve the equations without the scattering term $\bar{I}$. From Eq. (13), the corresponding

polarization can be solved as

$$P_\sigma(nk,n'k';t) = -\delta_{k'-k-q} g_q^{nn'} p_q^{Q_s} \bar{B}_s^\dagger(t)[f_{n\sigma}(k) - f_{n'\sigma}(k')] \times \left[e^{i(\omega_{kk'}^{nn'}+i0^+)t} - 1\right]/\left(\omega_{kk'}^{nn'} + i0^+\right). \quad (15)$$

Note that in the derivation, we have assumed that the SPP amplitude $\bar{B}_s$ varies slowly compared to the polarization P.

By substituting Eq. (15) into Eq. (12) and taking the long time limit $t \to \infty$, one gets

$$\partial_t \bar{B}_s/\bar{B}_s = -(\tau^{-1} + i\omega_s), \quad (16)$$

where ω_s represents the frequency shifting, expressed as

$$\omega_s = \sum_{nk,n'k',q\sigma} \left|p_q^{Q_s} g_q^{nn'}\right|^2 [f_{n'\sigma}(k') - f_{n\sigma}(k)] \frac{1}{\omega_{kk'}^{nn'}} \delta_{k'-k-q}, \quad (17)$$

in which the summation is understood as a principal value integral. τ^{-1} is the damping rate of the SPP, which has the form

$$\frac{1}{\tau} = \pi \sum_{nk,n'k',q\sigma} \left|p_q^{Q_s} g_q^{nn'}\right|^2 [f_{n'\sigma}(k') - f_{n\sigma}(k)] \delta\left(\omega_{kk'}^{nn'}\right) \delta_{k'-k-q}. \quad (18)$$

Note that Eq. (18) agrees with the Landau damping rate derived from the Fermi golden rule in the literature.[44,45]

The above solution suggests that the Landau damping process can be understood as the resonant absorption of the SPP by electrons. The two δ functions in Eq. (18) indicate that for a monochromatic SPP wave with wave vector q, the absorption occurs between pairs of states $|nk\rangle$ and $|n'k'\rangle$ satisfying the energy and momentum conservations

$$\omega_{kk'}^{nn'} = 0, \quad (19)$$

$$k' - k = q. \quad (20)$$

Each pair of the states $|nk\rangle$ and $|n'k'\rangle$ consist a resonant pair $(nk,n'k')$ relevant for the SPP damping. For the multisubband system, there usually exist several such resonant pairs, laying between different subbands n and n' and being well separated from each other. For a nonmonochromatic SPP wave packet with sufficiently narrow spectrum in q, the two states $|nk\rangle$ and $|n'k'\rangle$ of each resonant pair become two wave-vector regions. Note that in the following discussion, we shall focus on the nonmonochromatic SPP wave packet, and the resonant pair is referred to as the wave-vector region unless otherwise specified. The resonant pairs are illustrated in Figs. 2(a) and 2(b). By using the resonant pairs, one can rewrite Eq. (18) into

$$\tau^{-1} = \sum_i \tau_i^{-1}, \quad (21)$$

$$\tau_i^{-1} = \pi \sum_{q\sigma} \sum_{(nk,n'k')\in i} \left|p_q^{Q_s} g_q^{nn'}\right|^2 [f_{n'\sigma}(k') - f_{n\sigma}(k)] \times \delta\left(\omega_{kk'}^{nn'}\right) \delta_{k'-k-q}, \quad (22)$$

with i being the index for the resonant pair corresponding to the SPP wave packet, whose spectrum is decided by the line-shape function $p_q^{Q_s}$. $(nk,n'k') \in i$ means that the two states $|nk\rangle$ and $|n'k'\rangle$ belong to the ith resonant pair. Thus one can see that the damping rate of the SPP wave packet is the sum over the absorption rates of all the relevant resonant pairs.

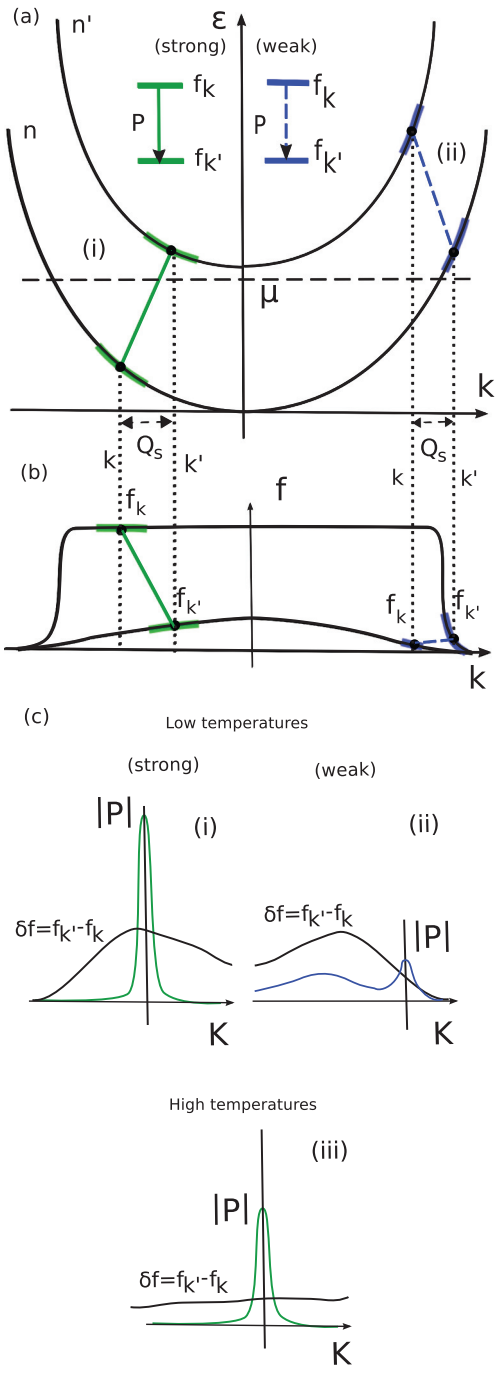

FIG. 2. (Color online) Schematic of the resonant pairs corresponding to the case of (i) strong and (ii) weak Landau damping in the electron spectrum (a) and in the electron distribution (b). The two wave-vector regions of the resonant pairs are illustrated by thick green/blue curves corresponding to the strong/weak Landau damping regime. The resonant pairs are centralized around the resonance corresponding to the SPP central wave vector Q_s as indicated by the vertical black dotted curves. The horizontal dashed line marks the chemical potential of the electrons μ. (c) The electron polarization and electron population difference as a function of the center wave vector $K = \frac{k+k'}{2}$ with $k' - k = Q_s$. (i)/(ii) corresponds to the strong/weak Landau damping regime at low temperatures and (iii) corresponds to both the strong and the weak Landau damping regimes at high temperatures. The vertical solid line marks the resonance corresponding to Q_s.

Note that the electron population difference $\delta f = f_{n'\sigma}(k') - f_{n\sigma}(k)$ of the corresponding resonant pair plays an important role on its contribution to the SPP damping. For the degenerate electrons where a well-defined Fermi surface exists around the chemical potential, there exist two regimes of the SPP damping: (i) a strong Landau damping regime where states $|nk\rangle$ and $|nk'\rangle$ of a resonant pair lay in each side of the chemical potential in the electron spectrum, leading to a large population difference δf and hence a strong SPP damping; (ii) a weak Landau damping regime where the chemical potential lies outside all the resonant pairs, leading to a small δf and a weak SPP damping. This is illustrated in Figs. 2(a) and 2(b). Note that at high enough temperatures, the Fermi surface can be smeared out and such difference vanishes.

It should be emphasized that according to Eq. (15), the resonant pair can be visualized as the resonant peak in the polarizations between the two subbands n and n'. In Fig. 2(c), we illustrate the polarizations $P(nk,n'k')$ corresponding to the resonant pairs shown in Figs. 2(a) and 2(b) as a function of the center wave vector $K = (k + k')/2$ with $k' - k = Q_s$. One finds that the polarization exhibits a Lorentzian peak around the resonance corresponding to the central wave vector Q_s, as indicated by Eq. (15).

Note that such resonant peak can show different features in the strong and weak Landau damping regimes at low temperatures. In the strong Landau damping regime, the corresponding polarization P exhibits a strong resonant peak concentrated in the region with large δf [(i) in Fig. 2(c)], indicating a large SPP absorption by the electrons. In contrast, in the weak Landau damping regime, the corresponding resonant peak is weak and lies outside the large δf region [(ii) in Fig. 2(c)], indicating a small SPP absorption. In addition to the resonant peak, side peaks can also exist in the off-resonant regime due to the corresponding large δf. At high temperatures where the Fermi surface is smeared out, the population difference is rather flat for both the strong and weak Landau damping regimes and the corresponding polarization exhibits a strong peak around the resonance for both regimes [(iii) in Fig. 2(c)].

D. Influence of the scattering

The scattering influences the Landau damping by changing the resonant excitation of the polarizations. Specifically, (1) the scattering can introduce dissipative channels, inducing a decay of the polarization; (2) the scattering between polarizations with different precession frequencies induces a frequency mixing, leading to a modification of the polarization precession frequency. These two effects can be further clarified by assuming that for each resonant pair, the scattering term has the form

$$\bar{I}^{i\sigma}_{nk,n'k'} = \sum_q \Gamma_i [P_\sigma(nk-q,n'k'-q) - P_\sigma(nk,n'k')], \quad (23)$$

where Γ_i stands for the phenomenological relaxation rate for the polarization of the ith resonant pair. Note that $(nk,n'k')$ and $(nk-q,n'k'-q)$ belong to the ith resonant pair.

For each resonant pair, the polarization P in the scattering term $\bar{I}$ given above can be obtained by treating Γ_i perturbatively and solving Eq. (13) order by order, yielding

$$P_\sigma(nk,n'k';t) = \delta_{k'-k-q} g_q^{nn'} p_q^{Q_s} \bar{B}_s^\dagger(t)[f_{n\sigma}(k) - f_{n'\sigma}(k')] \times \left[e^{i(\omega^{nn'}_{kk'} - \bar{\Gamma}^a_i + i\bar{\Gamma}^b_i)t} - 1\right] \Big/ \left(\omega^{nn'}_{kk'} - \bar{\Gamma}^a_i + i\bar{\Gamma}^b_i\right), \quad (24)$$

where

$$\bar{\Gamma}^b_i = \Gamma_i \sum_q \left(1 - \frac{\omega^{nn'}_{kk'}}{\omega^{nn'}_{k-q,k'-q}}\right), \quad (25)$$

$$\bar{\Gamma}^a_i = \pi\Gamma_i \sum_q \left(\omega^{nn'}_{kk'} - \omega^{nn'}_{k-q,k'-q}\right)\delta\left(\omega^{nn'}_{k-q,k'-q}\right). \quad (26)$$

The summation in Eq. (25) is understood as a principal value integral. Note that we have omitted the k,k' dependence of $\bar{\Gamma}^{a(b)}_i$ inside each resonant pair for simplicity. The detail of the derivation is given in Appendix C.

By comparing Eq. (24) to Eq. (15), one can see that the detuning $\omega^{nn'}_{kk'}$ in the resonant denominator is modified into $\omega^{nn'}_{kk'} - \bar{\Gamma}^a_i$, indicating that the polarization precession frequency is shifted by the scattering. The scattering also induces a finite imaginary part $\bar{\Gamma}^b_i$ to the resonant denominator, representing the decay of the polarization due to the scattering.

The above solution indicates that the scattering modifies the resonance between the polarization and the SPP by introducing both an energy shift and an energy broadening to the corresponding resonance pairs. On one hand, the energy shift modifies the energy conservation Eq. (19) into

$$\omega^{nn'}_{kk'} - \bar{\Gamma}^a_i = 0. \quad (27)$$

Thus the corresponding resonant pairs are shifted by the scattering. On the other hand, the energy broadening loosens the energy conservation constraint given by Eq. (19). Thus the corresponding resonant pairs are broadened. Note that the broadening and shifting are usually small and cannot induce overlaps between different resonant pairs.

Accordingly, the broadening $\bar{\Gamma}^b_i$ and shifting $\bar{\Gamma}^a_i$ also manifest themselves in the SPP damping rate. Following the same procedure as for the derivation of Eq. (18), the SPP damping rate in the presence of the scattering can be written as

$$\tau^{-1} = \sum_i \tau_i^{-1}, \quad (28)$$

$$\tau_i^{-1} = \sum_{q\sigma} \sum_{(nk,n'k')\in i} \left|p_q^{Q_s} g_q^{nn'}\right|^2 [f_{n'\sigma}(k') - f_{n\sigma}(k)] \times \frac{\bar{\Gamma}^b_i}{\left(\omega^{nn'}_{kk'} - \bar{\Gamma}^a_i\right)^2 + \left(\bar{\Gamma}^b_i\right)^2} \delta_{k'-k-q}. \quad (29)$$

By comparing the above equations to Eq. (18), one observes that the δ function corresponding to the energy conservation Eq. (19) is broadened into a Lorentzian with width $\bar{\Gamma}^b_i$ and shift $\bar{\Gamma}^a_i$.

It should be emphasized that the broadening and shifting of the resonance pair can also be visualized as the broadening and shifting of the corresponding resonant peak in the polarizations as illustrated in Fig. 3. This offers a simple way to interpret the influence of the broadening and shifting on the SPP damping rate. The influence of the shifting depends on the direction of the shift. From the figure, one can see that the shifting reduces

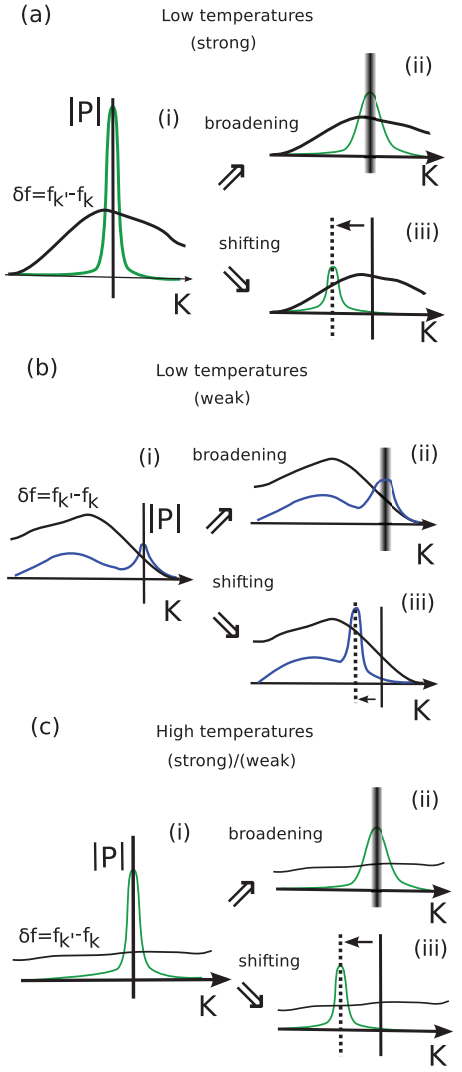

FIG. 3. (Color online) Schematic of the effect of the broadening and shifting on the electron polarization for (a) strong Landau damping regime at low temperatures, (b) weak Landau damping regime at low temperatures, and (c) both strong and weak Landau damping regimes at high temperatures. The thin solid vertical lines represent the resonance without broadening and shifting. The resonances with the broadening and shifting are represented by the thick solid and thin dotted vertical lines, respectively. For clarification, only the shifting towards the small K direction is illustrated. Note that the population differences δf become flat in both regimes at high temperatures.

the resonant peak in the polarization if the peak is shifted towards the region with smaller δf, thus the absorption of the SPP by the corresponding resonant pairs is reduced [(iii) in Figs. 3(a) and 3(c)] and the corresponding SPP damping rate is suppressed. Otherwise, if the peak is shifted towards the region with larger δf [(iii) in Fig. 3(b)], the absorption is enhanced and the SPP damping rate is enhanced.

The influence of the broadening can be different in the strong and weak Landau damping regimes at low temperatures as illustrated in Figs. 3(a) and 3(b). In the strong Landau damping regime, the broadening can reduce the sharp resonance peak of the polarization [(ii) in Fig. 3(a)] and suppress the absorption of the SPP. Thus the corresponding SPP damping rate is suppressed in this regime. In contrast, in the weak Landau damping regime, the broadening of the resonance increases the absorption from the region with larger δf [(ii) in Fig. 3(b)], thus the absorption is enhanced and the corresponding SPP damping rate is enhanced. Note that at high temperatures, as the polarization exhibits a sharp peak around the resonance in both the strong and weak Landau damping regimes, the scattering tends to suppress the SPP damping rate in both regimes [(ii) in Fig. 3(c)].

E. Broadening and shifting from a simplified model

In order to gain a further understanding of the microscopic origin of the broadening and shifting, we discuss the contributions of the ei, ep, and ee scatterings to the broadening and shifting within a simplified model in this section.

Within this model, we assume that the scattering only occurs between the polarizations inside each resonant pair. Under such assumption, all the scattering terms can be written in a unified form for the ith resonant pair:

$$\bar{I}^{i\sigma}_{nk,n'k'} = \sum_q \{\Gamma^a_{nk,n'k',i}(q)P_\sigma(nk-q,n'k'-q) - \Gamma^b_{nk,n'k',i}(q)P_\sigma(nk,n'k')\}, \tag{30}$$

where both $(nk,n'k')$ and $(nk-q,n'k'-q)$ belong to the ith resonant pair. Note that the corresponding $\Gamma^{a/b}$ for each scattering mechanism can be obtained by comparing the scattering terms [see Eqs. (B11)–(B13)] to $\bar{I}^{i\sigma}_{nk,n'k'}$ given in the above equation.

Note that Eq. (30) has a similar structure as Eq. (23), thus one can derive the corresponding broadening and shifting following a similar procedure, yielding

$$\bar{\Gamma}^b_i = \sum_q \left[\Gamma^b_{nk,n'k',i}(q) - \Gamma^a_{nk,n'k',i}(q)\frac{\omega^{nn'}_{kk'}}{\omega^{nn'}_{k-q,k'-q}}\right], \tag{31}$$

$$\bar{\Gamma}^a_i = \pi\sum_q \Gamma^a_{nk,n'k',i}(q)\left(\omega^{nn'}_{kk'} - \omega^{nn'}_{k-q,k'-q}\right)\delta\left(\omega^{nn'}_{k-q,k'-q}\right). \tag{32}$$

The broadening $\bar{\Gamma}^b_i$ and shifting $\bar{\Gamma}^a_i$ due to each scattering can be evaluated by substituting the corresponding scattering term into Eqs. (30)–(32). Note that we have omitted the k,k' dependence of $\bar{\Gamma}^{a(b)}_i$ inside each resonant pair to make the equation simple and physically transparent. For each resonant pair, $\bar{\Gamma}^{a(b)}_i$ is evaluated by choosing $(nk,n'k')$ corresponding to the SPP central wave vector Q_s (i.e., $k'-k=Q_s$) since the line-shape function $p^{Q_s}_q$ is peaked at $q=Q_s$. The shifting $\bar{\Gamma}^a_i$ can be written as

$$\bar{\Gamma}^{a(\mathrm{ei})}_i = 0, \tag{33}$$

$$\bar{\Gamma}^{a(\mathrm{ep})}_i = 0, \tag{34}$$

$$\bar{\Gamma}^{a(\mathrm{ee})}_i = 2\pi\sum_{j=1,2}\sum_{\bar{n}}\Pi^n_{n'}(\bar{n}\bar{k}_j,0), \tag{35}$$

where

$$\Pi^n_{n'}(\bar{n}\bar{k},q) = \sum_\sigma \tilde{V}^{n\bar{n}}_q\tilde{V}^{\bar{n}n'}_q f^{>}_{\bar{n}\sigma}(\bar{k}+q)f^{<}_{\bar{n}\sigma}(\bar{k}), \tag{36}$$

with $\tilde{V}_q$ being the screened ee interaction. $\bar{k}_1 = -2(\varepsilon^n_{k-Q_s} - \varepsilon^{n'}_{k'} + \Omega_s)/Q_s - Q_s/2$ and $\bar{k}_2 = 2(\varepsilon^n_k - \varepsilon^{n'}_{k'-Q_s} + \Omega_s)/Q_s + Q_s/2$. $\bar{\Gamma}^{a(\mathrm{ei})}_i$, $\bar{\Gamma}^{a(\mathrm{ep})}_i$, and $\bar{\Gamma}^{a(\mathrm{ee})}_i$ correspond to the contributions from the ei, ep, and ee scatterings, respectively. The corresponding broadenings have the forms

$$\bar{\Gamma}^{b(\mathrm{ei})}_i = m^*\pi n_i \left(\frac{\tilde{v}^{nn}_0}{|k|} - \frac{\tilde{v}^{n'n'}_0}{|k'|}\right)\left(\tilde{v}^{nn}_0 - \tilde{v}^{n'n'}_0\right), \tag{37}$$

$$\begin{aligned}\bar{\Gamma}^{b(\mathrm{ep})}_i = \sum_\sigma \Bigg\{ & \pi m^* \left(\sum_{\mathcal{Q}} M^{nn}_{\mathcal{Q},-q} M^{nn'}_{\mathcal{Q},-q}\right) \\ & \times [N^{>}_{\mathrm{LO}} f^{>}_{n\sigma}(k-q) + N^{<}_{\mathrm{LO}} f^{<}_{n\sigma}(k-q)]/|k-q||_{q=q^{(k)}_+} \\ & + \pi m^* \left(\sum_{\mathcal{Q}} M^{nn}_{\mathcal{Q},-q} M^{nn'}_{\mathcal{Q},-q}\right) \\ & \times [N^{<}_{\mathrm{LO}} f^{>}_{n\sigma}(k-q) + N^{>}_{\mathrm{LO}} f^{<}_{n\sigma}(k-q)]/|k-q||_{q=q^{(k)}_-} \Bigg\} \\ & + \{nk \longleftrightarrow n'k'\},\end{aligned} \tag{38}$$

$$\begin{aligned}\bar{\Gamma}^{b(\mathrm{ee})}_i = & \left\{ 2\pi \sum_{\bar{n}\bar{k}} \left[\Pi^n_n(\bar{n}\bar{k},0) - \Pi^n_{n'}(\bar{n}\bar{k},0)\right]/|k-\bar{k}| \right\} \\ & + \{nk \longleftrightarrow n'k'\},\end{aligned} \tag{39}$$

where $q^{(k)}_\pm$ satisfies $[q^{(k)}_\pm]^2 - 2kq_\pm \pm 2m^*\Omega_{\mathrm{LO}} = 0$ and $\tilde{v}^{nn'}_q$ represents the screened ei interaction. $\{nk \longleftrightarrow n'k'\}$ stands for the same term as in the previous {} but with the interchange of indices $nk \longleftrightarrow n'k'$.

From Eqs. (33)–(39), one finds that different scattering has different contribution to the broadening and shifting. Only the ee scattering contributes to the shifting, while the contributions from the ei and ep scatterings vanish. Although all the scatterings can contribute to the broadening, their relative importance can be quite different. This is because for the nanowires considered here, the ei, ep, and ee matrix elements $v^{nn'}_q$, $M^{nn'}_{\mathcal{Q}q}$ and $V^{nn'}_q$ are not sensitive to the subband index n. Thus, for the ei and ee scatterings, according to Eqs. (37) and (39), the terms in the bracket can largely cancel each other, leading to small contributions left. In contrast, such cancellation is absent for the ep scattering, thus its contribution to the broadening is expected to be larger than the ones from the ei and ee scatterings.

Equations (28) and (29) with the broadening and shifting given in Eqs. (33)–(39) consist the analytic solution for the SPP damping rate. The analytic solution in this section offers a simple picture to understand the influence of the scattering on the SPP damping: the SPP damping comes from the resonant absorption of the SPP by electrons, while the scattering can introduce a broadening and a shifting to the resonance and hence affects the damping process. At low temperatures, the broadening tends to suppress the SPP damping rate in the strong Landau damping regime. While in the weak Landau damping regime, the broadening tends to enhance the SPP damping. At high temperatures, such difference vanishes and the broadening tends to suppress the damping in both regimes. The shifting can suppress the SPP damping if the resonance is shifted towards the region with smaller δf, but boost it if the resonance is shifted toward the region with larger δf. Different scatterings can have different contributions to the broadening and shifting. From the simplified model in this section, one finds that the shifting is determined by the ee scattering, and the broadening is mainly decided by the ep scattering for the typical nanowires considered here.

III. NUMERICAL RESULTS

In the numerical investigation, we choose nanowires to be free-standing InAs nanowires. The typical electron density $\bar{n}_0$ is in the range of $10^{17} \sim 10^{18}$ cm^{-3} and the wire radius R is around $25 \sim 75$ nm.[74] The LO phonon energy $\Omega_{\mathrm{LO}} = 29$ meV and the electron effective mass $m^* = 0.023m_0$ with m_0 representing the free electron mass. The dielectric constants of the nanowires are $\epsilon^\infty_1 = 12.3$ for high frequency and $\epsilon^0_1 = 15.5$ for low frequency. The dielectric constant outside the nanowire is $\epsilon_2 = 1.0$. Note that for such nanowires, there are 10–20 electron subbands relevant to the SPP damping. We set the impurity line density $n_i = 0.5n_e$ with $n_e = \pi R^2 \bar{n}_0$ being the electron line density.

By numerical solving the kinetic equations Eqs. (12) and (13), one obtains the temporal evolution of the SPP amplitude $\bar{B}_s$. The SPP damping rate τ^{-1} can be extracted by fitting the real part of $\bar{B}_s$ with a single exponential decay of the cosine oscillation: $\mathrm{Re}[\bar{B}_s] = \bar{B}^0_s \exp(-t/\tau)\cos(\omega_s t)$, where the initial value of the SPP amplitude $\bar{B}^0_s$ is chosen to be real. We set the wave packet length $L = 100R$ (see Ref. 75).

A. Landau damping: size and temperature dependence

Before we discuss the influence of the scattering, it is helpful to first obtain an understanding of the SPP damping without scattering. In Fig. 4(a), we show a typical behavior of the SPP damping rate as a function of the SPP central wave vector Q_s and wire radius R for the nanowire with electron density $\bar{n}_0 = 1.5 \times 10^{17}$ cm^{-3}. The temperature is chosen to be 100 K. One finds that the SPP damping rate oscillates with the radius R. Note that similar size-dependent oscillations have also been reported in metal nanoparticles and thin films.[43–45,76–78]

Such oscillations are usually attributed to the quantized electron states in the nanostructures,[43–45] which can be understood in terms of the resonant pairs in the nanowires we studied here. To illustrate this, we concentrate on the damping rate corresponding to a typical SPP central wave vector $Q_s = 1.66 \times 10^{-2}$ nm^{-1} [skyblue curves in Fig. 4(a)] and show the corresponding resonant pairs for radii $R = 34$, 38.5, 40 and 43 nm in Fig. 4(b). Each resonant pair can be represented by the resonance corresponding to the central wave vector Q_s, since the line-shape function of the SPP wave packet is peaked at Q_s. There are four resonant pairs in Fig. 4(b) which lay between different subbands: pair (i) is between the subbands 1 and 4, pair (ii) is between the subbands 2 and 6, pair (iii) is between the subbands 3 and 9 and pair (iv) is between the subbands 4 and 8. In the figure, the four resonant pairs (i)–(iv) are denoted by the skyblue dots, green squares, brown open circles, and yellow triangles, respectively. The subbands corresponding to each resonant pair are also plotted with solid

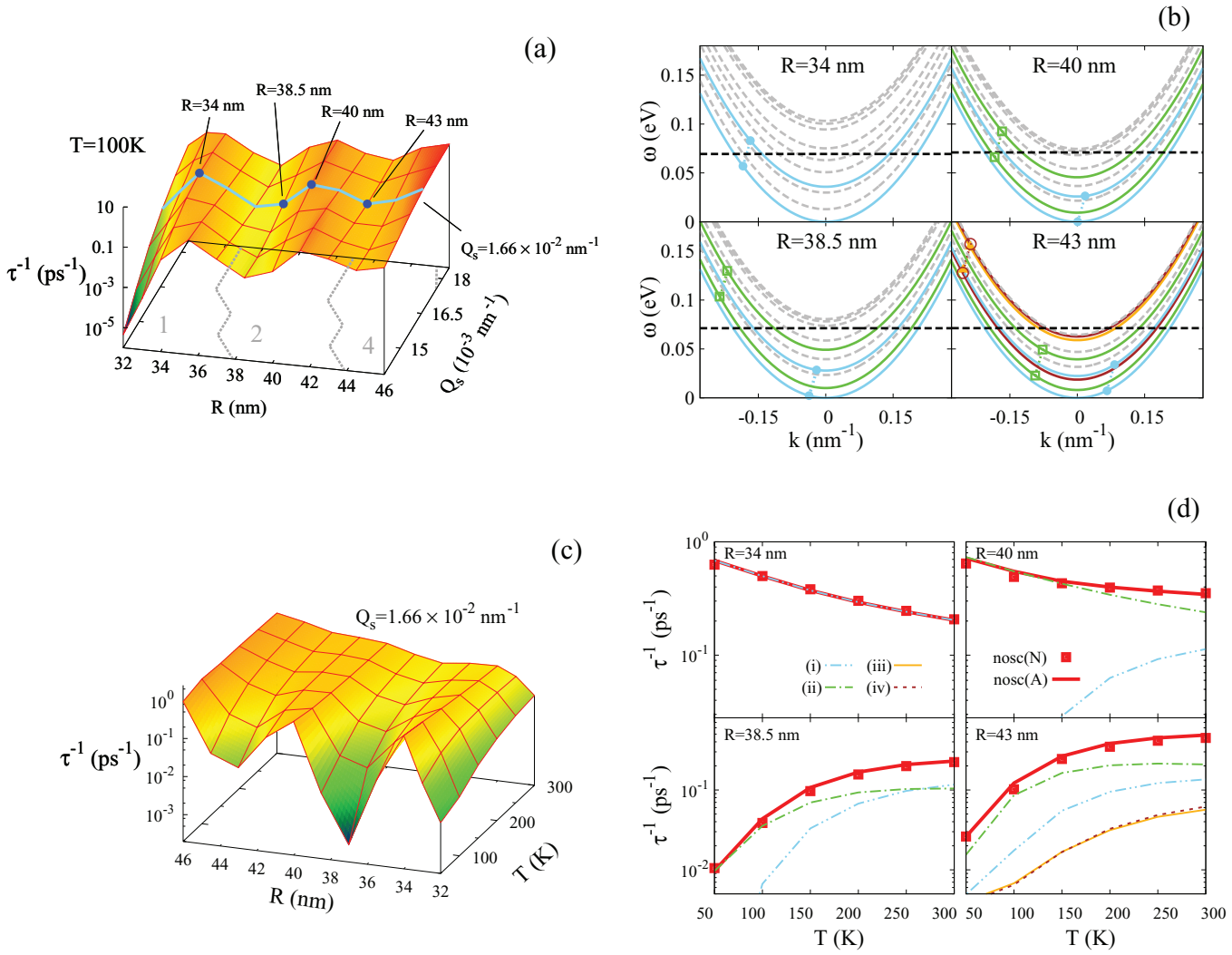

FIG. 4. (Color online) (a) The SPP damping rate as a function of SPP central wave vector Q_s and wire radius R without scattering for $\bar{n}_0 = 1.5 \times 10^{17}$ cm^{-3} and $T = 100$ K. The skyblue curve represents the damping rate corresponding to the SPP central wave vector $Q_s = 1.66 \times 10^{-2}$ nm^{-1}. The number of the relevant resonant pairs are labeled in the R-Q_s plane. (b) The resonant pairs for $R = 34$, 38.5, 40 and 43 nm corresponding to $Q_s = 1.66 \times 10^{-2}$ nm^{-1} in the electron spectrum. For clarification, only the lowest 10 subbands are plotted. (c) The SPP damping rate without scattering as a function of radius R and temperature T for $Q_s = 1.66 \times 10^{-2}$ nm^{-1}. (d) Temperature dependence of the damping rate τ^{-1} without scattering for $R = 34$, 38.5, 40, and 43 nm with $Q_s = 1.66 \times 10^{-2}$ nm^{-1}. Symbols correspond to the numerical results. Red curves represent the results from the analytic solution. The contributions of each resonant pair from the analytic solution are also plotted as curves with different colors. The skyblue double-dotted chain, green chain, brown dotted, and yellow solid curves correspond to the contribution from the resonant pairs (i)–(iv), respectively.

curves in the same color. Note that for $R = 34$ nm, only the resonant pair (i) is relevant for the damping. For $R = 38.5$ and 40 nm, both the resonant pairs (i) and (ii) are relevant. For $R = 43$ nm, all the four resonant pairs (i)–(iv) contribute to the SPP damping.

From Fig. 4(b), one can see that as the radius R increases, the resonant pairs move from left to right in the electron spectrum. When a resonant pair moves across the chemical potential marked by the horizontal black dashed lines, a crossover between the strong and weak Landau damping regimes occurs, which induces the size-dependent oscillations shown in Fig. 4(a). Note that the peaks/valleys correspond to the strong/weak Landau damping regimes. For example, the oscillation from $R = 32$ to 38.5 nm is due to the crossover induced by the resonant pair (i). While the crossover induced by the resonant pair (ii) induces the oscillation from $R = 38.5$ to 43 nm. One finds from the figure that $R = 34$ and 40 nm correspond to the strong Landau damping regime whereas $R = 38.5$ and 43 nm correspond to the weak Landau damping regime.

One also observes from Fig. 4(b) that due to the many subbands in the nanowires, there usually exist multiresonant pairs relevant for the SPP damping. For a given Q_s, more and more resonant pairs become involved as the radius R increases. The number of relevant resonant pairs are labeled in the R-Q_s plane in Fig. 4(a). Note that as the number of the resonant pairs increases, the magnitude of the size-dependent oscillations becomes less pronounced. This is mainly because the oscillations are usually induced by the crossover due to one resonant pair as R varies. For the system with

many resonant pairs, the contribution from one resonant pair becomes less significant. Thus the size-dependent oscillations can be suppressed for nanowires with large R.

It should be emphasized that the size-dependent oscillations can also be suppressed by increasing temperature T. This is because the crossover is more pronounced for strongly degenerate electrons where a clear Fermi surface exists around the chemical potential. In high-temperature regime, the crossover is largely suppressed. To show this, we plot the damping rate τ^{-1} as a function of the radius R and temperature T for $Q_s = 1.66 \times 10^{-2}$ nm^{-1} in Fig. 4(c). One sees that as temperature increases, the damping rate τ^{-1} corresponding to the strong Landau damping regime decreases, while τ^{-1} corresponding to the weak Landau damping regime increases. This leads to a suppression of the size-dependent oscillations in high-temperature regime.

One can also obtain the above results from the analytic solution of the kinetic equations without scattering [see Eqs. (21) and (22)]. To show this, we compare the temperature dependence of τ^{-1} from both the numerical (red squares) and analytic (red solid curves) solutions for the nanowires with $R = 34$, 38.5, 40, and 43 nm in Fig. 4(d). One finds good agreement between each other, indicating that the analytic solution without scattering offers a good estimation to the numerical results. Note that according to the analytic solution, the temperature dependence of the SPP damping rate originates from the population difference of the resonant pairs.

From the analytic solution, one can also identify contributions from different resonant pairs, which are plotted as curves with different colors and line shapes in Fig. 4(d). The skyblue double-dotted chain, green chain, brown dotted and yellow solid curves correspond to the contributions from the resonant pairs (i)–(iv), respectively. It is clear that the relative importance of the resonant pairs can be quite different. For the strong Landau damping regime, there usually exists one resonant pair whose contribution is much larger than the other pairs. For example, the damping rate τ^{-1} is mainly determined by the resonant pairs (i) and (ii) for $R = 34$ and 40 nm, respectively. For the weak Landau damping regime, the contributions from different resonant pairs can be comparable. For example, for $R = 38.5$ and 43 nm, although the resonant pair (ii) has a large contribution to the damping rate τ^{-1}, the other resonant pairs can also play important roles, especially at high temperatures.

From the above results, one finds that the SPP damping exhibits size-dependent oscillations and distinct temperature dependence without scattering, which can be explained by the analytic solution.

B. Influence of scattering

Now we discuss the influence of the scattering on the SPP damping. In Fig. 5(a), we plot the damping rate τ^{-1} as a function of the radius R and temperature T for $Q_s = 1.66 \times 10^{-2}$ nm^{-1} in the presence of all the scattering. Comparing to the case without scattering [see Fig. 4(c)], one finds that the scattering has pronounced influence on the SPP damping: (1) the size-dependent oscillations are effectively smeared out and (2) the temperature dependence also becomes weaker compared to the case without scattering.

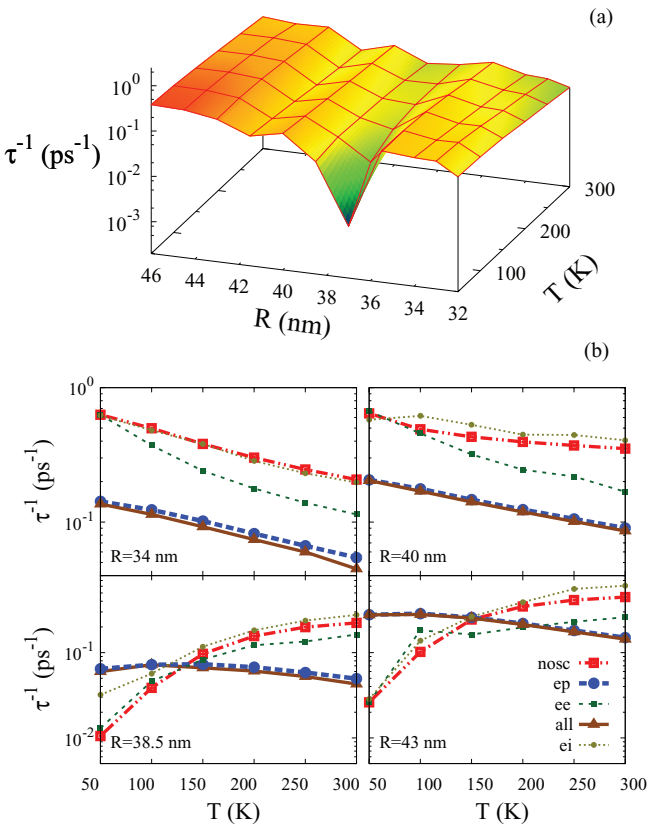

FIG. 5. (Color online) (a) SPP damping rate in the presence of all the scattering as a function of radius R and temperature T for $Q_s = 1.66 \times 10^{-2}$ nm^{-1}. (b) SPP damping rate τ^{-1} calculated from the numerical results for $Q_s = 1.66 \times 10^{-2}$ nm^{-1} with different scattering for $R = 34$, 38.5, 40, and 43 nm. Symbols with big blue dots, small green squares, small olive dots represent τ^{-1} calculated with the ep, ee, and ei scatterings, respectively. The brown triangles represent τ^{-1} calculated in the presence of all the three scatterings and the red squares represent τ^{-1} without scattering.

To gain a better understanding of the influence of the scattering, in Fig. 5(b), we compare the temperature dependence of the damping rate τ^{-1} with and without scattering for nanowires with four typical radii $R = 34$, 38.5, 40, and 43 nm. The brown triangles represent τ^{-1} calculated in the presence of all the three scatterings, while τ^{-1} without scattering are plotted with red squares for comparison. Note that $R = 34$ and 40 nm correspond to the strong Landau damping regime, whereas $R = 38.5$ and 43 nm correspond to the weak one.

In the presence of the scattering, it is seen that the damping rate τ^{-1} is markedly suppressed in the strong Landau damping regime ($R = 34$ and 40 nm). In contrast, for the weak Landau damping regime ($R = 38.5$ and 43 nm), the scattering plays different roles in different temperature regimes: The damping rate is markedly enhanced in the low-temperature regime ($T \lesssim 150$ K), but is largely suppressed in the high-temperature regime ($T \gtrsim 150$ K). A crossover exists at the intermediate temperature regime. It is also noted that the damping rate can be enhanced/suppressed by almost one order of magnitude by the scattering.

To understand these influences, we first identify the dominant scattering mechanism. To do so, we calculate the damping

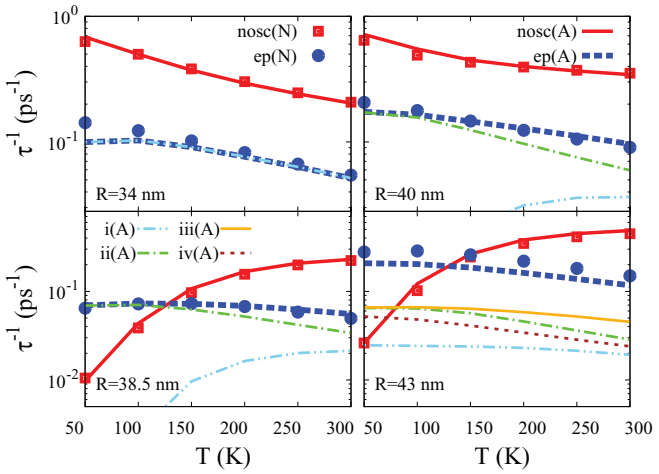

FIG. 6. (Color online) Comparison between the numerical and analytical results of the SPP damping rate for $R = 34$, 38.5, 40, and 43 nm with the ep scattering. Blue dots represent the numerical results, while the blue dashed curves show the results from the analytic solution. The contribution of each resonant pair from the analytic solution is also plotted. The skyblue double-dotted chain, green chain, brown dotted, and yellow solid curves correspond to the contribution from the resonant pairs (i)–(iv), respectively. For comparison, the numerical and analytical results for the damping rate without scattering are also plotted with red squares and solid curves, respectively.

rates τ^{-1} with the ep, ee, or ei scattering only, and plot them with big blue dots, small green squares and small olive dots in Fig. 5(b), respectively. It is clear to see from the figure that the damping rate τ^{-1} is dominated by the ep scattering.[79]

We first concentrate on the ep scattering. From the analytic solution within the simplified model, we have attributed the effect of the ep scattering to the broadening of the resonant pairs. To see if this picture gives a proper description of the influence of the ep scattering in general case, we calculate the temperature dependence of the damping rate τ^{-1} by using the analytic solution Eqs. (28) and (29) with the ep-scattering-induced broadening given in Eq. (38). The calculated analytic results are compared to the numerical ones in Fig. 6.

In the figure, the blue dots represent the damping rate τ^{-1} from the numerical results, while the blue dashed curves represent τ^{-1} from the analytic results. For comparison, we also plot the numerical and analytic results without scattering with red squares and solid curves, respectively. One finds good agreement between each other, indicating that the broadening can give a proper description of the effect of the ep scattering. Note that at low temperatures, the broadening tends to suppress the SPP damping rate in the strong Landau damping regime ($R = 34$ and 40 nm), while in the weak Landau damping regime ($R = 38.5$ and 43 nm), the broadening tends to enhance the SPP damping rate. At high temperatures, such difference vanishes and the SPP damping rate is suppressed in both the strong and weak Landau damping regimes. This leads to a crossover between the suppression and enhancement for $R = 38.5$ and 43 nm corresponding to the weak Landau damping regime as shown in Fig. 6. This also agrees with the conclusion from the analytic solution.

It is worth noting that the scattering can also suppress the temperature dependence of the SPP damping rate. This is because the temperature dependence originates from the population difference of the resonant pairs. For the resonant pairs with the broadening, the corresponding population difference is less sensitive to the temperature, leading to the suppression of the temperature dependence of the corresponding SPP damping rate.

We further point out that the scattering can also change the relative importance of different resonant pairs. To see this, we identify contributions of different resonant pairs from the analytic solution, as applied in Sec. III A for the case without scattering. In Fig. 6, the skyblue double-dotted chain, green chain, brown dotted, and yellow solid curves correspond to the contributions from the resonant pairs (i)–(iv), respectively. One finds that the resonant pair (i) dominates the damping for $R =$ 34 nm, whereas the resonant pair (ii) plays the most important role for $R = 38.5$ and 40 nm. For $R = 43$ nm, all the four resonant pairs have comparable contributions to the damping, with the largest contribution coming from the resonant pair (iii). Comparing to the case without scattering [see Fig. 4(d)], one also finds that the relative importance of different resonant pairs is modified by the broadening, especially in weak Landau damping regime.

From the above discussion, one comes to the conclusion that the influence of the ep scattering on the SPP damping rate can be understood as the broadening of the resonant pairs. The analytic solution incorporating such broadening shows good agreement with the numerical result. Note that in the above results, the contribution of the SO phonons is omitted since it is much smaller than that from the LO phonons. This is shown in detail in Appendix D.

Now we briefly address the ee and ei scatterings. From the analytic solution within the simplified model, the effect of the ei scattering is attributed to the broadening of the resonant pairs. While for the ee scattering, the main effect is due to the shifting. The SPP damping rate with the ee/ei scattering can also be calculated from the analytic solution [see Eqs. (28) and (29) with the broadening and shifting given in Eqs. (33) and (37) for the ei scattering and Eqs. (35) and (39) for the ee scattering, respectively]. The analytic results are compared to the numerical ones in Fig. 7. From the figure, one observes qualitatively good agreement between each other, indicating that the ee and ei scatterings can also be understood as the broadening and/or shifting of the resonant pairs.

It is pointed out that the effect of the broadening and shifting can be visualized from the behavior of the polarization, which gives a more intuitive picture for the effect of the scattering. This is discussed in detail in Appendix E.

From the above results, one finds that the scattering tends to smear out the size-dependent oscillations of the SPP damping rate. The temperature dependence can also be suppressed by the scattering. Note that this effect is quite general and can be seen for nanowires with different electron densities. To demonstrate this, we show the size and temperature dependence of the SPP damping rates for nanowires with electron density $\bar{n}_0 = 5.0 \times 10^{17}\ \mathrm{cm}^{-3}$ without and with scattering in Figs. 8(a) and 8(b), respectively. The central wave vector of the SPP wave packet is chosen to be $Q_s = 1.3 \times 10^{-2}\ \mathrm{nm}^{-1}$. From the figure, it is seen that the size-dependent oscillations are smeared

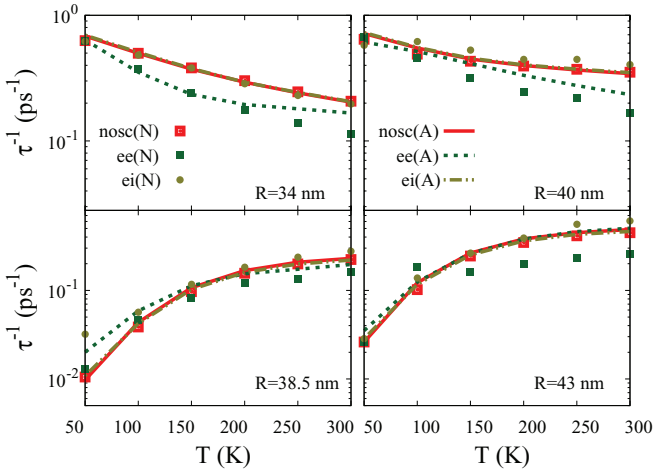

FIG. 7. (Color online) Comparison between the numerical and analytical results of the SPP damping rate for the ee and ei scatterings for $R = 34$, 38.5, 40, and 43 nm. Small green squares and green dotted curves represent the numerical and analytical results for the ee scattering, respectively. Small olive dots and olive double-dotted chain represent the numerical and analytical results for the ei scattering, respectively. For comparison, the numerical and analytical results for the damping rate without scattering are also plotted with red squares and solid curves, respectively.

out by the scattering. The temperature dependence is also suppressed. These effects are similar to the ones for nanowires with $\bar{n}_0 = 1.5 \times 10^{17}$ cm^{-3} investigated above, indicating that these effects are quite general for typical InAs nanowires.

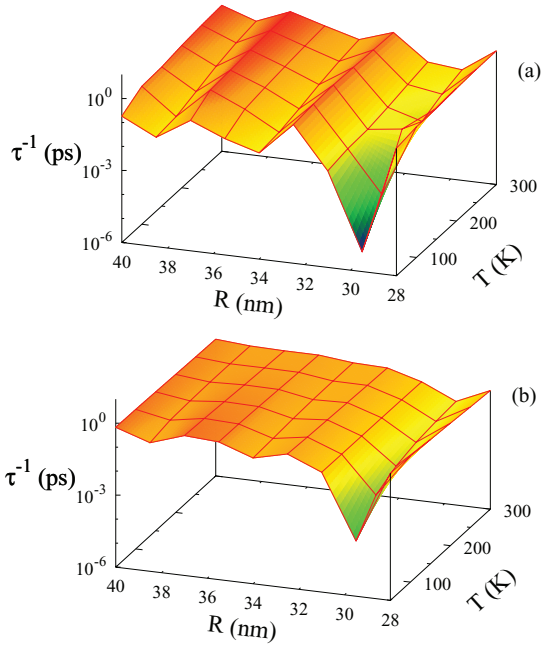

FIG. 8. (Color online) Size and temperature dependence of the SPP damping rate for nanowires with electron density $\bar{n}_0 = 5.0 \times 10^{17}$ cm^{-3} (a) without any scattering and (b) with all the scattering. The central wave vector of the SPP wave packet is chosen to be $Q_s = 1.3 \times 10^{-2}$ nm^{-1}.

IV. CONCLUSION AND DISCUSSION

In conclusion, we present a microscopic kinetic theory to study the effect of the electron scattering on the Landau damping of the SPP in semiconductor nanowires. Based on the semiclassical model Hamiltonian of the SPP-electron system and the nonequilibrium Green-function approach, we derive the kinetic equations of the SPP-electron system, with all the scattering explicitly included. Within this model, the SPP damping is understood as the absorption of the SPP by the electron polarization of the resonant pairs. The population difference of the resonant pairs δf plays an important role on the SPP damping, leading to a strong and a weak Landau damping regimes for degenerate electrons. The scattering influences the SPP damping via the broadening and shifting of the resonant pairs, which have different effects on the strong and weak Landau damping regimes. At low temperatures, the broadening tends to suppress the SPP damping in the strong Landau damping regime. Whereas in the weak Landau damping regime, the broadening tends to enhance the SPP damping. At high temperatures, this difference tends to be vanished. The shifting can suppress the SPP damping if the resonance is shifted towards the region with smaller δf, but boost it if the resonance is shifted toward the region with larger δf. The broadening and shifting can be visualized from the corresponding electron polarization of the resonant pairs. Moreover, different scattering has different contribution to the broadening and shifting. The main effect of the ei/ep scattering is to cause a broadening, whereas the main effect of the ee scattering is to introduce a shifting. The effect of the broadening and shifting can be incorporated into an analytic solution, which shows good agreement with the numerical result.

To demonstrate the effect of the scattering, we investigate the damping of the axial symmetric SPP mode in InAs nanowires in the presence of the ei, ee, and ep scatterings. Without any scattering, the SPP damping exhibits size-dependent oscillations and a distinct temperature dependence. In the presence of the scattering, the size-dependent oscillations are markedly smeared out and the temperature dependence is also suppressed. The damping rate can be enhanced/suppressed by almost one order of magnitude. For InAs nanowires investigated here, the ep scattering is found to be dominant. These results are found to be general for typical InAs nanowires, which demonstrate the importance of the scattering on the SPP damping for semiconductor nanowires. It is further pointed out that our model can be applied to nanowires made of other semiconductors, offering a systematic way to investigate the effect of electron scattering on the SPP damping in such systems.

ACKNOWLEDGMENTS

This work was supported by the National Basic Research Program of China under Grant No. 2012CB922002 and the Strategic Priority Research Program of the Chinese Academy of Sciences under Grant No. XDB01000000. One of the authors (Y.Y.) was also partially supported by the China Postdoctoral Science Foundation.

APPENDIX A: SEMICLASSICAL MODEL FOR SPP

Our derivation of the quantized SPP Hamiltonian $H_{\rm SPP}$ and its coupling to electrons $H_{\text{SPP-el}}$ follows the procedure used in Ref. 80, in which the SPPs are obtained from quantization of the classical plasmon field. The classical plasmon field is derived within the hydrodynamical model, which treats plasmons as irrotational deformations of the conduction electrons.[80–84] From this model, the Hamiltonian of the plasmon can be written as[80]

$$\begin{aligned} H_{\rm SPP} = & \int d\boldsymbol{r}\frac{m^*}{2}n(\boldsymbol{r})|\nabla\eta(\boldsymbol{r})|^2 \\ & + \frac{e^2}{2}\int d\boldsymbol{r}\frac{e^2}{2}\int d\boldsymbol{r}' n(\boldsymbol{r})n(\boldsymbol{r}')V_{\rm ee}(\boldsymbol{r},\boldsymbol{r}') \\ & + \int d\boldsymbol{r}G[n(\boldsymbol{r})], \end{aligned} \tag{A1}$$

where the irrotational flow has been assumed, i.e., $\boldsymbol{v}(\boldsymbol{r}) = \nabla\eta(\boldsymbol{r})$ with $\boldsymbol{v}(\boldsymbol{r})$ being the velocity field. $n(\boldsymbol{r})$ is the electron density and m^* represents the electron effective mass.

For both $\boldsymbol{r}$ and $\boldsymbol{r}'$ inside the nanowire, the Coulomb interaction $V_{\rm ee}(\boldsymbol{r},\boldsymbol{r}')$ has the form[85]

$$\begin{aligned} V_{\rm ee}(\boldsymbol{r},\boldsymbol{r}') = & \frac{e}{4\pi\epsilon_1^\infty}\left\{\frac{1}{|\boldsymbol{r}-\boldsymbol{r}'|}+\frac{2}{\pi}\left(\frac{\epsilon_1^\infty}{\epsilon_2}-1\right)\right. \\ & \times\sum_{m=-\infty}^{+\infty}e^{im(\varphi-\varphi')}\int_0^\infty dk\cos[k(z-z')] \\ & \left.\times\ \mathbb{C}_m\left(kR,\frac{\epsilon_1^\infty}{\epsilon_2}\right)I_m(k\rho)I_m(k\rho')\right\}, \end{aligned} \tag{A2}$$

where

$$\mathbb{C}_m\left(kR,\frac{\epsilon_1^\infty}{\epsilon_2}\right) = \frac{K_m(kR)K_m'(kR)}{I_m(kR)K_m'(kR)-\frac{\epsilon_1^\infty}{\epsilon_2}I_m'(kR)K_m(kR)}. \tag{A3}$$

Note that the distortion of the Coulomb interaction $V_{\rm ee}(\boldsymbol{r},\boldsymbol{r}')$ by the dielectric mismatch between the nanowire and the environment has been taken into account, which is not addressed in previous work.

$G[n(\boldsymbol{r})]$ represents the exchange, correlation and internal energy of the electrons, which is approximated by the Thomas-Fermi functional

$$G[n(\boldsymbol{r})] = \frac{3}{10m^*}(3\pi^2)^{2/3}n^{5/3}(\boldsymbol{r}), \tag{A4}$$

with the exchange-correlation contributions neglected.

From the above Hamiltonian, up to the first order of the perturbation, one can derive linearized hydrodynamic equations as

$$\partial_t n_1(\boldsymbol{r}) = \nabla\cdot[n_0(\boldsymbol{r})\nabla\eta_1(\boldsymbol{r})], \tag{A5}$$

$$\partial_t\eta_1(\boldsymbol{r}) = \frac{e}{m^*}\int d\boldsymbol{r}'V_{\rm ee}(\boldsymbol{r},\boldsymbol{r}')n_1(\boldsymbol{r}')+\frac{5\gamma}{3m^*}\frac{n_1(\boldsymbol{r})}{[n_0(\boldsymbol{r})]^{1/3}}, \tag{A6}$$

where n_1 and η_1 are perturbations around the equilibrium. $n_0(\boldsymbol{r}) = \bar{n}_0\Theta(R-\rho)$ is the electron density in the equilibrium with $\bar{n}_0$ being the average electron density, $\gamma = \frac{(3\pi)^{2/3}}{5m^*}$.

The normal modes from the above equations include both the surface plasmon and volume plasmon modes. The surface modes, which we focus on in this paper, can be represented by the ansatz[83]

$$\eta_{qm}(\boldsymbol{r}) = R\sum_q \dot{Q}_{qm}e^{im\varphi+iqz}[I_m(q\rho)+AI_m(\kappa\rho)], \tag{A7}$$

where $I_m(\rho)$ is the modified Bessel function of the first kind. A and κ are parameters depending on m and q, with m being the angular quantum number of the SPP mode and q representing the SPP wave vector along the wire axis. Here, the first term in the square bracket represents the incompressible deformation of the electrons, while the second term represents the correction due to the finite compressibility.

By substituting the ansatz Eq. (A7) into Eqs. (A5) and (A6), one obtains the equation for the parameter κ:

$$\begin{aligned} & 1-\frac{\beta^2}{\omega_p^2}(\kappa^2-q^2)-(qR)I_{m+1}(qR)K_m(qR) \\ & \quad\times\left\{\mathbb{C}_{qm}'\left(\frac{\kappa R}{qR}\frac{I_{m+1}(\kappa R)}{I_{m+1}(qR)}-\frac{I_m(\kappa R)}{I_m(qR)}\right)\right. \\ & \quad+\left[\frac{\kappa R}{qR}\frac{I_{m+1}(\kappa R)}{I_{m+1}(qR)}A(1+\mathbb{C}_{qm}')\right. \\ & \quad\left.\left.-A\left(\frac{\kappa R}{qR}\frac{I_{m+1}(\kappa R)}{I_{m+1}(qR)}+\frac{I_m(\kappa R)}{I_{m+1}(qR)}\frac{K_{m+1}(qR)}{K_m(qR)}\right)\right]\right\} \\ & = 0, \end{aligned} \tag{A8}$$

with $\omega_p = \sqrt{\frac{e^2\bar{n}_0}{m^*\epsilon_1^\infty}}$ being the bulk plasma frequency and $\beta = \sqrt{\frac{5\gamma}{3m^*}\bar{n}_0^{2/3}}$. The parameter A can be expressed as

$$A = -\frac{I_{m+1}(qR)(qR)(1+\mathbb{C}_{qm}')}{I_{m+1}(\kappa R)(\kappa R)\left[1+\mathbb{C}_{qm}'\frac{(qR)I_{m+1}(qR)I_m(\kappa R)}{(\kappa R)I_{m+1}(\kappa R)I_m(qR)}\right]}, \tag{A9}$$

where

$$\mathbb{C}_m'(qR) = \frac{\frac{\epsilon_1^\infty}{\epsilon_2}-1}{1+\frac{\epsilon_1^\infty}{\epsilon_2}\frac{I_{m+1}(qR)}{I_m(qR)}\frac{K_m(qR)}{K_{m+1}(qR)}}. \tag{A10}$$

Once κ is obtained, the corresponding eigenfrequency Ω_{qm} can be calculated from the equation

$$\begin{aligned} & 1+\beta^2\frac{\kappa^2-q^2}{\Omega_{qm}^2}-\frac{\omega_p^2}{\Omega_{qm}^2}\left\{1-\left(\frac{\epsilon_1^\infty}{\epsilon_2}-1\right)\mathbb{C}_m(qR)\right. \\ & \quad\left.\times[(\kappa R)I_{m+1}(\kappa R)I_m(qR)-(qR)I_m(\kappa R)I_{m+1}(qR)]\right\} \\ & = 0. \end{aligned} \tag{A11}$$

Note that without the dielectric mismatch ($\epsilon_1^\infty = \epsilon_2$), Eqs. (A8)–(A11) agree with the results for the surface mode from Ref. 83.

The Hamiltonian of the SPP can be obtained by substituting Eq. (A7) into Eq. (A1) and keeping only terms up to the linear order, which can be written as

$$H = \frac{2\pi R^3m^*\bar{n}_0}{2}\sum_{qm}\left[|\dot{Q}_{qm}'|^2+\Omega_{qm}^2|Q_{qm}'|^2\right], \tag{A12}$$

where the canonical coordinate Q'_{qm} has the form

$$Q'_{qm} = \sqrt{[AI_m(\kappa R)\kappa + I_m(qR)q]} \times \sqrt{[AI_m(\kappa R) + I_m(qR)]}Q_{qm}. \quad \text{(A13)}$$

Following the canonical quantization procedure, the collective coordinate Q'_{qm} can be transformed into

$$Q'_{qm} = \sqrt{\frac{1}{2\pi R^3 m^* \bar{n}_0 \Omega_{qm}}}(b_{qm} + b^\dagger_{-qm}), \quad \text{(A14)}$$

where the annihilation(creation) operator $b_{qm}(b^\dagger_{qm})$ satisfies the boson commutation relation $[b_{qm}, b^\dagger_{q'm'}] = \delta_{q,q'}\delta_{mm'}$. Substituting Eq. (A14) into Eq. (A12), the Hamiltonian of the SPP is quantized as

$$H_{\rm SPP} = \sum_{qm} \frac{\Omega_{qm}}{2}(2b^\dagger_{qm}b_{qm} + 1). \quad \text{(A15)}$$

By choosing $m = 0$, one obtains the Hamiltonian of the axial symmetric SPP mode under investigation:

$$H_{\rm SPP} = \sum_q \Omega_q b^\dagger_q b_q, \quad \text{(A16)}$$

without taking into account the zero-point energy, which is irrelevant for our study. The angular quantum number m is also omitted without confusion.

Following a similar procedure, the induced potential of the SPP mode can be quantized as

$$V^{\rm in}(\rho,\varphi,z) = \int dq\, \tilde{V}^{\rm in}_q(\rho,\varphi,z)(b_q + b^\dagger_{-q}), \quad \text{(A17)}$$

where

$$\tilde{V}^{\rm in}_q(\rho,\varphi,z) = -\frac{e^2}{2\pi\epsilon_1^\infty}\sqrt{\frac{\bar{n}_0}{2\pi m^*\omega_p}}\frac{e^{iqz}}{\sqrt{\Omega_q}} \times \frac{I_0(q\rho)\mathcal{C}''_q + AI_0(\kappa\rho)}{\sqrt{[AI_1(\kappa R)\kappa R + I_1(qR)qR][AI_0(\kappa R) + I_0(qR)]}} \quad \text{(A18)}$$

with

$$\mathcal{C}''_q = -[(\kappa R)AI_1(\kappa R) + (qR)I_1(qR)][K_0(qR) + \mathbb{C}'_0(qR)K_0(qR)] + A\Big[(\kappa R)I_1(\kappa R)K_0(qR) + (qR)I_0(\kappa R)K_1(qR) + \mathbb{C}'_0(qR)K_0(qR)\Big((\kappa R)I_1(\kappa R) - (qR)I_0(\kappa R)\frac{I_1(qR)}{I_0(qR)}\Big)\Big]. \quad \text{(A19)}$$

The SPP-electron coupling Hamiltonian $H_{\text{SPP-el}}$ in Eq. (9) can be obtained by combining the single-electron states in Eq. (5) and the induced potential of the SPP given above. The corresponding matrix element reads

$$g^{nn'}_{k-k'} = \int \rho d\rho d\varphi dz \psi^*_{nk}(\rho,\varphi,z)\tilde{V}^{\rm in}_{k-k'}(\rho,\varphi,z)\psi_{n'k'}(\rho,\varphi,z), \quad \text{(A20)}$$

with ψ_{nk} given in Eq. (5).

Now let us discuss the matrix elements for the interaction Hamiltonians for electrons. For the ei interaction, we have assumed that the impurities are distributed on the surface of the nanowire with an axially symmetric distribution.[74] Given the electron wave function ψ_{nk} in Eq. (5), the corresponding matrix element $v^{nn'}_q$ can be calculated as

$$v^{nn'}_q = \frac{e^2\delta_{\tilde{m}\tilde{m}'}}{2\pi^2\epsilon_1^\infty R}\int_0^1 d\bar{\rho}\bar{\rho}\frac{J_{\tilde{m}}(\lambda^{\tilde{m}}_{\tilde{n}}\bar{\rho})J_{\tilde{m}'}(\lambda^{\tilde{m}'}_{\tilde{n}'}\bar{\rho})}{J_{\tilde{m}+1}(\lambda^{\tilde{m}+1}_{\tilde{n}})J_{\tilde{m}'+1}(\lambda^{\tilde{m}'+1}_{\tilde{n}'})} \times [I_0(qR\bar{\rho})K_0(qR) + \mathbb{C}'_0(qR)I_0(qR\bar{\rho})K_0(qR)]. \quad \text{(A21)}$$

Note that the dielectric mismatch effect has been taken into account in the above expression. For the ep interaction, we here consider the polar interaction between the electrons and the LO phonons. The corresponding matrix element reads

$$M^{nn'}_{\boldsymbol{Q}q} = \frac{\sqrt{2\pi e^2\Omega_{\rm LO}(1/\epsilon_1^\infty - 1/\epsilon_1^0)}}{J_{\tilde{m}+1}(\lambda^{\tilde{m}}_{\tilde{n}})J_{\tilde{m}'+1}(\lambda^{\tilde{m}'}_{\tilde{n}'})}\frac{2}{|\boldsymbol{q}|} \times \int_0^1 d\bar{\rho}\bar{\rho}J_{\tilde{m}}(\lambda^{\tilde{m}}_{\tilde{n}}\bar{\rho})J_{\tilde{m}'}(\lambda^{\tilde{m}'}_{\tilde{n}'}\bar{\rho})e^{i\bar{\rho}\boldsymbol{Q}\cdot\boldsymbol{e}_\rho R}\delta_{\tilde{m}\tilde{m}'}, \quad \text{(A22)}$$

where $\boldsymbol{q} = (\boldsymbol{Q}, q)$ represents the LO phonon wave vector and $\Omega_{\rm LO}$ is the LO phonon energy. $\boldsymbol{e}_\rho$ is the unit vector along the radial direction of the wire and ϵ_1^0 is the dielectric constant of the nanowire in the static limit. Note that here we model the LO phonons by 3D modes, which is adequate for nanowires with large diameter.[68,69] For the ee Coulomb interaction, the corresponding matrix element reads

$$V^{nn'}_q = \frac{2e^2}{\pi\epsilon_1^\infty}\int_0^1 d\bar{\rho}_1\bar{\rho}_1\int_0^1 d\bar{\rho}_2\bar{\rho}_2\Big[I_0(qR\bar{\rho}_<)K_0(qR\bar{\rho}_>) + \left(\frac{\epsilon_1^\infty}{\epsilon_2} - 1\right)I_0(qR\bar{\rho}_1)I_0(qR\bar{\rho}_2)\mathbb{C}_0\left(qR, \frac{\epsilon_1^\infty}{\epsilon_2}\right)\Big] \times \left[\frac{J_{\tilde{m}}(\lambda^{\tilde{m}}_{\tilde{n}}\bar{\rho}_1)}{J_{\tilde{m}+1}(\lambda^{\tilde{m}}_{\tilde{n}})}\frac{J_{\tilde{m}'}(\lambda^{\tilde{m}'}_{\tilde{n}'}\bar{\rho}_2)}{J_{\tilde{m}'+1}(\lambda^{\tilde{m}'}_{\tilde{n}'})}\right]^2, \quad \text{(A23)}$$

where $\rho_> = \max(\rho_1,\rho_2)$ and $\rho_< = \min(\rho_1,\rho_2)$. Here we have omitted the interband term of the Coulomb interaction which can be small for nanostructures.[86] Note that the dielectric mismatch effect has been taken into account in the ee Coulomb interaction.

APPENDIX B: DERIVATION OF KINETIC EQUATIONS

The time evolution of $B_q(t) = \langle b_q(t)\rangle$ can be derived from the Heisenberg equation of the annihilation operator b_q, which reads

$$\partial_t B_q(t) = -i\Omega_q B_q(t) + \sum_{nn',kk',\sigma} p^{Q_s}_{k-k'} g^{nn'}_{k-k'} G^<_\sigma(n'k',nk;tt). \quad \text{(B1)}$$

By using the definitions of $\bar{B}_s$ and P given below Eq. (14), one has

$$\partial_t \bar{B}_s(t) = -i \sum_q \left(\Omega_{Q_s+q} - \Omega_s\right) p_q^{Q_s} B_{Q_s+q} e^{i\Omega_s t} - i \sum_{nn'\sigma} \sum_{kk'} p_{k-k'}^{Q_s} g_{k-k'}^{nn'} [P_\sigma(nk,n'k';t)]^\dagger, \quad \text{(B2)}$$

where the first term in the right-hand side of the equation describes the effect of the SPP dispersion on the dynamics of the SPP wave packet and the second term describes the dissipative effect due to the coupling to electrons. For the SPP wave packet with sufficiently large length L, the line-shape function $p_q^{Q_s}$ exhibits a sharp symmetric peak around the central wave vector Q_s. In this case, one can perform the Taylor expansion of the dispersive relation Ω_{Q_s+q} around Q_s up to the linear order of q to eliminate the first term. In doing so, we omit the effect of the SPP dispersion on the wave packet dynamics and consider only the dissipative effect.

Within the nonequilibrium Green-function approach, the quantum kinetic equation of electrons can be derived following the Kadanoff-Baym method,[66,67] yielding

$$\left[-i\partial_t - \left(\varepsilon_{k'}^{n'} - \varepsilon_k^n\right)\right] G_\sigma^{\gtrless}(nk,n'k';tt) = \sum_{\bar{n}q} (B_{-q} + B_q^\dagger)\left[g_q^{\bar{n}n'} G_\sigma^{\gtrless}(nk,\bar{n}k'-q;tt) - g_q^{n\bar{n}} G_\sigma^{\gtrless}(\bar{n}k+q,n'k';tt)\right] + I_{nk,n'k'}^{\gtrless\sigma}(t), \quad \text{(B3)}$$

where the first term in the right-hand side of the equation is the coherent driving term of electrons by the SPP and the second term describes the scattering

$$I_{nk,n'k'}^{\gtrless\sigma}(t) = \int_{-\infty}^{t} d\bar{t} \sum_{\bar{k}} \{[\Sigma^{\lessgtr}(k\bar{k};t\bar{t}) G_\sigma^{\gtrless}(\bar{k}k';\bar{t}t) - G_\sigma^{\gtrless}(k\bar{k};t\bar{t})\Sigma^{\lessgtr}(\bar{k}k';\bar{t}t))] - [> \longleftrightarrow <]\}, \quad \text{(B4)}$$

where $[> \longleftrightarrow <]$ stands for the same term as in the previous [] but with the interchange of $> \longleftrightarrow <$. It should be emphasized that due to the driving of the SPP, the dressed Green function $G_\sigma^{\gtrless}$ has off-diagonal components with respect to the momentum k and subband index n.

By treating the driving term as a perturbation, the kinetic equation can be linearized by keeping only terms up to the linear order,

$$\left[-i\partial_t - \left(\varepsilon_{k'}^{n'} - \varepsilon_k^n\right)\right] G_\sigma^{\gtrless}(nk,n'k';tt) = (B_{k-k'} + B_{k'-k}^\dagger)\left[g_{k'-k}^{nn'} G_{0\sigma}^{\gtrless}(nk,nk;tt) - g_{k'-k}^{nn'} G_{0\sigma}^{\gtrless}(n'k',n'k';tt)\right] + I_{nk,n'k'}^{\gtrless\sigma}(t). \quad \text{(B5)}$$

The first term in the right-hand side of the equation is the linearized driving term. Note that within the linearization, the dressed Green function $G_\sigma^{\gtrless}$ in the driving term is replaced by the free-electron Green function $G_{0\sigma}^{\gtrless}$, which is diagonal with respect to the momentum k and subband index n. By using the definition $P_\sigma(nk,n'k';t) = -iG_\sigma^<(nk,n'k';tt)e^{i\Omega_s t}$ and $f_{n\sigma}(k) = -iG_{0\sigma}^<(nk,nk;tt)$, one obtains Eq. (13) from the above equation.

Now we turn to the scattering term. We first discuss the ei scattering. Following the standard approximation,[66] the corresponding scattering term can be expressed as

$$I_{nk,n'k'}^{\mathrm{ei},\sigma} = -[S_{\mathrm{ei},\sigma}(nk,n'k';>,<) - S_{\mathrm{ei},\sigma}^\dagger(n'k',nk;<,>)] + [> \longleftrightarrow <], \quad \text{(B6)}$$

$$S_{\mathrm{ei},\sigma}(nk,n'k';>,<) = \int_{-\infty}^{t} d\bar{t} \sum_{\bar{n}\bar{n}'\bar{n}} \sum_{\tilde{k}q} n_i \tilde{v}_q^{n\bar{n}} \tilde{v}_q^{\bar{n}\bar{n}'} \times G_\sigma^{>}(\bar{n}k-q,\bar{n}'\tilde{k}-q;t\bar{t}) G_\sigma^{<}(\tilde{n}\tilde{k},n'k';\bar{t}t), \quad \text{(B7)}$$

where $\tilde{v}_q^{nn'} = v_q^{nn'}/\epsilon^{nn'}(q)$ is the screened electron-impurity interaction. The screening $\epsilon^{nn'}(q)$ is evaluated following Ref. 87 in the static limit, which can be written as

$$\epsilon^{nn'}(q) = 1 - \sum_{l\sigma} \frac{V_q^{nl} V_q^{ln'}}{V_q^{nn'}} \sum_k \frac{f_{l\sigma}(k+q) - f_{l\sigma}(k)}{\varepsilon_{k+q}^l - \varepsilon_k^l - i0^+}. \quad \text{(B8)}$$

Note that $S_{\mathrm{ei},\sigma}$ contains the product of two dressed Green functions. By keeping only terms up to the linear order, $S_{\mathrm{ei},\sigma}$ can be linearized as

$$S_{\mathrm{ei},\sigma}(nk,n'k';>,<) = \int_{-\infty}^{t} d\bar{t} \sum_{\bar{n}\bar{n}} \sum_{\tilde{k}q} n_i \tilde{v}_q^{n\bar{n}} \tilde{v}_q^{\bar{n}\bar{n}} \times G_{0\sigma}^{>}(\bar{n}k-q,\bar{n}k-q;t\bar{t}) G_\sigma^{<}(\tilde{n}k,n'k';\bar{t}t) + \int_{-\infty}^{t} d\bar{t} \sum_{\bar{n}\bar{n}'} \sum_{\tilde{k}q} n_i \tilde{v}_q^{n\bar{n}} \tilde{v}_q^{n'\bar{n}'} \times G_\sigma^{>}(\bar{n}k-q,\bar{n}'k'-q;t\bar{t}) G_{0\sigma}^{<}(n'k',n'k';\bar{t}t). \quad \text{(B9)}$$

Note that within the linearization, $S_{\mathrm{ei},\sigma}$ is separated into two terms. Each term contains only one dressed Green function $G_\sigma^{\gtrless}$, while the other one is replaced by the free Green function $G_{0\sigma}^{\gtrless}$. By applying the rotating wave approximation with respect to the SPP frequency Ω_s, one can remove the non-frequency-matched terms in the above equation, yielding

$$S_{\mathrm{ei},\sigma}(nk,n'k';>,<)e^{-i\Omega_s t} = \pi n_i \sum_{\bar{n}\bar{n}'q} \delta\left(\varepsilon_{k-q}^{\bar{n}} - \varepsilon_{k'}^{n'} + \Omega_s\right) \times \left[v_q^{n\bar{n}} v_q^{\bar{n}\bar{n}'} f_{\bar{n}\sigma}^{>}(k-q) P_\sigma(\bar{n}'k,n'k') - v_q^{n\bar{n}} v_q^{\bar{n}'n'} f_{n'\sigma}^{<}(k') P_\sigma(\bar{n}k-q,\bar{n}'k'-q)\right] \quad \text{(B10)}$$

in the Markovian limit. Substituting Eq. (B10) into Eqs. (B6) and (B7) and using the definition $\bar{I}_{nk,n'k'}^{\sigma} = I_{nk,n'k'}^{\sigma} e^{i\Omega_s t}$, one gets the final expression of the impurity scattering term:

$$\bar{I}_{nk,n'k'}^{\mathrm{ei},\sigma} = \pi n_i \sum_{\bar{n}\bar{n}'q} \left\{\delta\left(\varepsilon_{k-q}^{\bar{n}} - \varepsilon_{k'}^{n'} + \Omega_s\right) \times \left[\tilde{v}_q^{n\bar{n}} \tilde{v}_q^{\bar{n}'n'} P_\sigma(\bar{n}k-q,\bar{n}'k'-q) - \tilde{v}_q^{n\bar{n}} \tilde{v}_q^{\bar{n}\bar{n}'} P_\sigma(\bar{n}'k,n'k')\right] + \delta\left(\varepsilon_{k'-q}^{\bar{n}'} - \varepsilon_k^n - \Omega_s\right) \times \left[\tilde{v}_q^{n\bar{n}} \tilde{v}_q^{\bar{n}'n'} P_\sigma(\bar{n}k-q,\bar{n}'k'-q) - \tilde{v}_q^{\bar{n}\bar{n}'} \tilde{v}_q^{\bar{n}'n'} P_\sigma(nk,\bar{n}k')\right]\right\}. \quad \text{(B11)}$$

The ep scattering term can be derived following a similar procedure, which reads

$$\begin{aligned}\bar{I}^{\mathrm{ph},\sigma}_{nk,n'k'} = \pi \sum_{\bar{n}\bar{n}'} \sum_{q\,\boldsymbol{Q}} \big\{ & \delta\big(\varepsilon^{\bar{n}}_{k+q} - \varepsilon^{n'}_{k'} + \Omega_s + \Omega_{\mathrm{LO}}\big)\big[M^{n\bar{n}}_{\boldsymbol{Q}q} M^{\bar{n}'n'}_{\boldsymbol{Q}q} (N^{>}_{\mathrm{LO}} f^{<}_{n'\sigma}(k') + N^{<}_{\mathrm{LO}} f^{>}_{n'\sigma}(k')) P_\sigma(\bar{n}k+q,\bar{n}'k'+q) \\ & - M^{n\bar{n}}_{\boldsymbol{Q}q} M^{\bar{n}n'}_{\boldsymbol{Q}q} (N^{>}_{\mathrm{LO}} f^{>}_{\bar{n}\sigma}(k+q) + N^{<}_{\mathrm{LO}} f^{<}_{\bar{n}\sigma}(k+q)) P_\sigma(\bar{n}'k,n'k')\big] + \delta\big(\varepsilon^{\bar{n}}_{k+q} - \varepsilon^{n'}_{k'} + \Omega_s - \Omega_{\mathrm{LO}}\big)\big[M^{n\bar{n}}_{\boldsymbol{Q}q} M^{\bar{n}'n'}_{\boldsymbol{Q}q} (N^{<}_{\mathrm{LO}} f^{<}_{n'\sigma}(k') \\ & + N^{>}_{\mathrm{LO}} f^{>}_{n'\sigma}(k')) P_\sigma(\bar{n}k+q,\bar{n}'k'+q) - M^{n\bar{n}}_{\boldsymbol{Q}q} M^{\bar{n}n'}_{\boldsymbol{Q}q} (N^{<}_{\mathrm{LO}} f^{>}_{\bar{n}\sigma}(k+q) + N^{>}_{\mathrm{LO}} f^{<}_{\bar{n}\sigma}(k+q)) P_\sigma(\bar{n}'k,n'k')\big] \\ & + \delta\big(\varepsilon^{\bar{n}'}_{k'+q} - \varepsilon^{n}_{k} - \Omega_s + \Omega_{\mathrm{LO}}\big)\big[M^{n\bar{n}}_{\boldsymbol{Q}q} M^{\bar{n}'n'}_{\boldsymbol{Q}q} (N^{>}_{\mathrm{LO}} f^{<}_{n\sigma}(k) + N^{<}_{\mathrm{LO}} f^{>}_{n\sigma}(k)) P_\sigma(\bar{n}k+q,\bar{n}'k'+q) \\ & - M^{n'\bar{n}'}_{\boldsymbol{Q}q} M^{\bar{n}\bar{n}'}_{\boldsymbol{Q}q} (N^{>}_{\mathrm{LO}} f^{>}_{\bar{n}'\sigma}(k'+q) + N^{<}_{\mathrm{LO}} f^{<}_{\bar{n}'\sigma}(k'+q)) P_\sigma(nk,\bar{n}k')\big] \\ & + \delta\big(\varepsilon^{\bar{n}'}_{k'+q} - \varepsilon^{n}_{k} - \Omega_s - \Omega_{\mathrm{LO}}\big)\big[M^{n\bar{n}}_{\boldsymbol{Q}q} M^{\bar{n}'n'}_{\boldsymbol{Q}q} (N^{<}_{\mathrm{LO}} f^{<}_{n\sigma}(k) + N^{>}_{\mathrm{LO}} f^{>}_{n\sigma}(k)) P_\sigma(\bar{n}k+q,\bar{n}'k'+q) \\ & - M^{n'\bar{n}'}_{\boldsymbol{Q}q} M^{\bar{n}\bar{n}'}_{\boldsymbol{Q}q} (N^{<}_{\mathrm{LO}} f^{>}_{\bar{n}'\sigma}(k'+q) + N^{>}_{\mathrm{LO}} f^{<}_{\bar{n}'\sigma}(k'+q)) P_\sigma(nk,\bar{n}k')\big]\big\}, \end{aligned} \tag{B12}$$

where $N^{<(>)}_{\mathrm{LO}} = N_{\mathrm{LO}} + \frac{1}{2} - (+)\frac{1}{2}$ with $N_{\mathrm{LO}} = 1/[\exp(\frac{\Omega_{\mathrm{LO}}}{k_B T}) - 1]$ representing the thermal LO phonon distribution. The ee scattering term can also be derived in a similar way:

$$\begin{aligned}\bar{I}^{\mathrm{ee},\sigma}_{nk,n'k'} = 2\pi \sum_{q\bar{n}\bar{k}} \big\{ & \delta\big(\varepsilon^{n}_{k-q} - \varepsilon^{n'}_{k'} + \Omega_s + \varepsilon^{\bar{n}}_{\bar{k}+q} - \varepsilon^{\bar{n}}_{\bar{k}}\big)\big[f^{<}_{n'\sigma}(k') \Pi^{n}_{n'}(\bar{n}\bar{k},q) P_\sigma(nk-q,n'k'-q) - f^{>}_{n\sigma}(k-q) \Pi^{n}_{n}(\bar{n}\bar{k},q) P_\sigma(nk,n'k')\big] \\ & + \delta\big(\varepsilon^{n}_{k-q} - \varepsilon^{n'}_{k'} + \Omega_s + \varepsilon^{\bar{n}}_{\bar{k}} - \varepsilon^{\bar{n}}_{\bar{k}-q}\big)\big[f^{>}_{n'\sigma}(k') \Pi^{n'}_{n}(\bar{n}\bar{k},-q) P_\sigma(nk-q,n'k'-q) - f^{<}_{n\sigma}(k-q) \Pi^{n}_{n}(\bar{n}\bar{k},-q) P_\sigma(nk,n'k')\big] \\ & + \delta\big(\varepsilon^{n}_{k} - \varepsilon^{n'}_{k'-q} + \Omega_s + \varepsilon^{\bar{n}}_{\bar{k}} - \varepsilon^{\bar{n}}_{\bar{k}+q}\big)\big[f^{<}_{n\sigma}(k) \Pi^{n}_{n'}(\bar{n}\bar{k},q) P_\sigma(nk-q,n'k'-q) - f^{>}_{n'\sigma}(k'-q) \Pi^{n'}_{n'}(\bar{n}\bar{k},q) P_\sigma(nk,n'k')\big] \\ & + \delta\big(\varepsilon^{n}_{k} - \varepsilon^{n'}_{k'-q} + \Omega_s + \varepsilon^{\bar{n}}_{\bar{k}-q} - \varepsilon^{\bar{n}}_{\bar{k}}\big)\big[f^{>}_{n\sigma}(k) \Pi^{n'}_{n}(\bar{n}\bar{k},-q) P_\sigma(nk-q,n'k'-q) - f^{<}_{n'\sigma}(k'-q) \Pi^{n'}_{n'}(\bar{n}\bar{k},-q) P_\sigma(nk,n'k')\big]\big\}, \end{aligned} \tag{B13}$$

where $\Pi^{n}_{n'}(\bar{n}\bar{k},q) = \sum_\sigma \tilde{V}^{n\bar{n}}_q \tilde{V}^{\bar{n}n'}_q f^{>}_{\bar{n}\sigma}(\bar{k}+q) f^{<}_{\bar{n}\sigma}(\bar{k})$ with $\tilde{V}^{nn'}_q = V^{nn'}_q/\epsilon^{nn'}(q)$ being the screened ee interaction.

APPENDIX C: SCATTERING-INDUCED FREQUENCY MODIFICATION AND DECAY OF THE POLARIZATION

The polarization P for the ith resonant pair in the presence of the scattering term $\bar{I}^{\sigma}_{nk,n'k'}$ given in Eq. (23) can be solved by treating Γ_i as perturbation and solve Eq. (13) order by order. By assuming

$$P_\sigma(nk,n'k') = \sum_{j=0}^{\infty} P^{(j)}_\sigma(nk,n'k';t), \tag{C1}$$

one obtains

$$\partial_t P^{(0)}_\sigma(nk,n'k') = i\omega^{nn'}_{kk'} P^{(0)}_\sigma(nk,n'k';t) + i g^{nn'}_{k-k'} p^{Q_s}_{k-k'} \bar{B}^{\dagger}_s [f_{n\sigma}(k) - f_{n'\sigma}(k')], \tag{C2}$$

for zeroth order and

$$\partial_t P^{(j+1)}_\sigma(nk,n'k') = i\omega^{nn'}_{kk'} P^{(j+1)}_\sigma(nk,n'k';t) + \sum_q \Gamma_i \big[P^{(j)}_\sigma(nk-q,n'k'-q) - P^{(j)}_\sigma(nk,n'k')\big], \tag{C3}$$

for $(j+1)$th order, with $j \geqslant 0$.

In the long-time limit $t \to \infty$, the solution of the above equations reads

$$P^{(0)}_\sigma(nk,n'k') = -g^{nn'}_{k-k'} p^{Q_s}_{k-k'} \bar{B}^{\dagger}_s [f_{n\sigma}(k) - f_{n'\sigma}(k')]/\big(\omega^{nn'}_{kk'} + i0^+\big), \tag{C4}$$

for zeroth order, and

$$P^{(j+1)}_\sigma(nk,n'k') = \frac{P^{(j)}_\sigma(nk,n'k')}{\omega^{nn'}_{kk'} + i0^+} i\Gamma_i \sum_q \left[\frac{P^{(j)}_\sigma(nk-q,n'k'-q)}{P^{(j)}_\sigma(nk,n'k')} - 1\right], \tag{C5}$$

for $(j+1)$th order.

Now let us evaluate $\sum_q [\frac{P^{(j)}_\sigma(nk-q,n'k'-q)}{P^{(j)}_\sigma(nk,n'k')} - 1]$. For zeroth order,

$$\begin{aligned}\sum_q \left[\frac{P^{(0)}_\sigma(nk-q,n'k'-q)}{P^{(0)}_\sigma(nk,n'k')} - 1\right] &= \sum_q \left[\frac{g^{nn'}_{k-k'} p^{Q_s}_{k-k'} \bar{B}^{\dagger}[f_{n\sigma}(k) - f_{n'\sigma}(k')]}{g^{nn'}_{k-k'} p^{Q_s}_{k-k'} \bar{B}^{\dagger}[f_{n\sigma}(k-q) - f_{n'\sigma}(k'-q)]} \frac{\omega^{nn'}_{kk'}}{\omega^{nn'}_{k-q,k-q'} + i0^+} - 1\right] \\ &\approx \sum_q \left[\frac{\omega^{nn'}_{kk'}}{\omega^{nn'}_{k-q,k-q'} + i0^+} - 1\right], \end{aligned} \tag{C6}$$

where we have assumed that $f_{n\sigma}(k)$ varies slowly with respect to k and can be canceled out. The first-order term can be evaluated as

$$\begin{aligned}
&\sum_q \left[\frac{P_\sigma^{(1)}(nk-q,n'k'-q)}{P_\sigma^{(1)}(nk,n'k')}-1\right] \\
&= \sum_q \left\{\sum_{q'}\left[P_\sigma^{(0)}(nk-q-q',n'k'-q-q')-P_\sigma^{(0)}(nk-q,n'k'-q)\right]\left\{\sum_q\left[P_\sigma^{(0)}(nk-q,n'k'-q)\right.\right.\right. \\
&\quad \left.\left.\left.-\ P_\sigma^{(0)}(nk,n'k')\right]\right\}^{-1}\frac{\omega_{kk'}^{nn'}}{\omega_{k-q,k-q'}^{nn'}+i0^+}-1\right\} \\
&\approx \sum_q\left[\frac{\omega_{kk'}^{nn'}}{\omega_{k-q,k-q'}^{nn'}+i0^+}-1\right], \qquad \text{(C7)}
\end{aligned}$$

where we have assumed that $\sum_q[P_\sigma^{(0)}(nk-q,n'k'-q)-P_\sigma^{(0)}(nk,n'k')]$ varies slowly with respect to $k(k')$ and can be cancelled out.

Following a similar procedure, for jth order, one has

$$\sum_q\left[\frac{P_\sigma^{(j)}(nk-q,n'k'-q)}{P_\sigma^{(j)}(nk,n'k')}-1\right]\approx\sum_q\left[\frac{\omega_{kk'}^{nn'}}{\omega_{k-q,k-q'}^{nn'}+i0^+}-1\right], \qquad \text{(C8)}$$

with $j\geqslant 1$.

By combining Eqs. (C1), (C4)–(C6), and (C8), one obtains Eqs. (24)–(26).

APPENDIX D: EFFECT OF THE SO PHONONS

The SO phonons in nanowires[69] can also influence the damping of the SPP. However, for the typical InAs nanowires we considered here, the SO phonons are of marginal importance since their contribution is much smaller than that from the LO phonons. This will be shown in this Appendix.

The induced potential due to the SO phonon is given by[88–90]

$$V_{\rm SO}=\sum_p\left(\Gamma_p^{\rm SO}e^{iqz}e^{ip\varphi}a_p^{\rm SO}+\text{H.c.}\right), \qquad \text{(D1)}$$

with

$$\Gamma_p^{\rm SO}=\sqrt{\frac{2\pi e^2R}{q}\frac{D(\Omega_{\rm SO})}{I_p(qR)I_p'(qR)}}I_p(qr), \qquad \text{(D2)}$$

$$D(\omega)=\frac{\epsilon_2(\omega)}{\epsilon_2(\omega)\frac{\partial}{\partial\omega}\epsilon_1(\omega)-\epsilon_1(\omega)\frac{\partial}{\partial\omega}\epsilon_2(\omega)}, \qquad \text{(D3)}$$

$$\epsilon_i(\omega)=\epsilon_i^\infty\frac{\Omega_{\rm Li}^2-\omega^2}{\Omega_{\rm Ti}^2-\omega^2}, \qquad \text{(D4)}$$

where $a_p^{\rm SO}$ is the annihilation operator for the SO phonons and $\Omega_{\rm SO}$ is the SO phonon energy. $\Omega_{\rm Li}(\Omega_{\rm Ti})$ represents the LO(TO) phonon energy inside ($i=1$) and/or outside ($i=2$) the nanowire. The coordinates are chosen according to Fig. 1(a).

As the SO phonon energy is very close to the LO phonon energy for typical InAs nanowires,[69] we assume $\Omega_{\rm SO}=\Omega_{\rm LO}$ in the calculation. By using the single electron states in Eq. (5), the corresponding electron-SO-phonon interaction Hamiltonian can be written as

$$H_{\rm SO}=\sum_{pq}\sum_{nn'k\sigma}\bar{M}_{pq}^{nn'}\left[a_{pq}^{\rm SO}+\left(a_{-p-q}^{\rm SO}\right)^\dagger\right]c_{nk\sigma}^\dagger c_{n'k-q\sigma}, \qquad \text{(D5)}$$

where the interaction matrix element reads

$$\begin{aligned}
\bar{M}_{pq}^{nn'}&=\frac{\sqrt{\pi e^2\Omega_{\rm SO}\left(1/\epsilon_1^\infty-1/\epsilon_1^0\right)R/q}}{J_{\tilde{m}+1}\left(\lambda_{\tilde{n}}^{\tilde{m}}\right)J_{\tilde{m}'+1}\left(\lambda_{\tilde{n}'}^{\tilde{m}'}\right)}\delta_{\tilde{m},\tilde{m}'+p} \\
&\quad\times\int_0^1 d\bar{\rho}\,\bar{\rho}\,J_{\tilde{m}}\left(\lambda_{\tilde{n}}^{\tilde{m}}\bar{\rho}\right)J_{\tilde{m}'}\left(\lambda_{\tilde{n}'}^{\tilde{m}'}\bar{\rho}\right)\frac{I_p(qR\bar{\rho})}{\sqrt{I_p(qR)I_p'(qR)}}. \qquad \text{(D6)}
\end{aligned}$$

By using the analytic solution given in Secs. II D and II E, we calculate the temperature dependence of the SPP damping rates for $R=34$ and 38.5 nm in the presence of the ep scattering with and without the contribution of the SO phonons, which is plotted in Fig. 9. One can see that the damping rates are dominated by the LO phonons, and the SO phonons have very little effect.

APPENDIX E: VISUALIZATION OF THE BROADENING AND SHIFTING

We have seen that the SPP damping rate can be understood as the broadening and shifting of the resonant pairs. In the analytic solution, the broadening and shifting can be seen clearly from both the resonant denominator in the polarization [see Eq. (24)] and the Lorentzian in the damping rate [see Eq. (29)]. One may wonder whether the broadening and shifting can also be observed in a more intuitive way from the numerical results. In fact, inspired by Eq. (24), the broadening and shifting of the resonant pairs can be visualized from the normalized polarization $P(nk,n'k')/(\delta f\,\bar{B}_s)$, from which the structure of the resonant denominator can be identified.

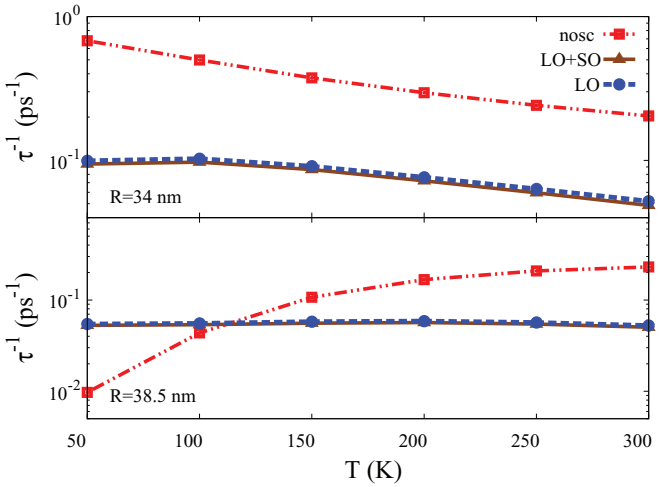

FIG. 9. (Color online) Temperature dependence of SPP damping rate in the presence of the ep scattering for $R = 34$ and 38.5 nm. Blue dashed curves represent the results with only the LO phonon scattering, while the brown solid curves represent the results with both the LO and SO phonon scatterings. The damping rates without any scattering are plotted with red double-dotted chain curves for comparison. Other parameters are all the same as Fig. 6.

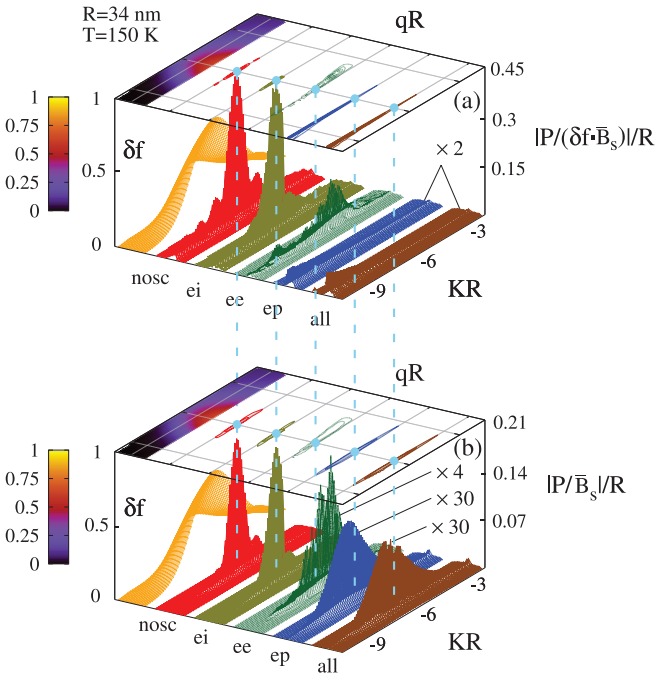

FIG. 10. (Color online) 3D plot and the corresponding contour plot of the normalized (a) and unnormalized (b) electron polarization corresponding to the resonant pair (i) for $R = 34$ nm, $T = 150$ K. The corresponding population difference is also plotted in the figure. The olive, green, and blue curves represent the polarization with the ei, ee, and ep scattering only, respectively. The red curves represent the polarization without scattering, while the brown curves represent the polarization in the presence of all the three scatterings. In the contour plots, the resonance corresponding to the SPP central wave vector Q_s is shown with a skyblue dot in the contour plot. The population difference is plotted with orange curves. Different curves are offset along q axis for clarity. To provide a clear visualization, in (a) the normalized polarizations with the ep and all the scatterings are enlarged by a factor of 2. In (b), the unnormalized polarization with the ee/ep/all scattering is enlarged by a factor of 4/30/30.

Before we show the numerical results of the normalized polarizations, we first explain what we expect from the polarizations. According to the analytic solution Eq. (15), the magnitude of the normalized polarization $|P(nk,n'k')/(\delta f\ \bar{B}_s)|$ without scattering can exhibit a sharp Lorentzian peak around the resonance corresponding to the SPP central wave vector Q_s as indicated by the resonant denominator. Several side peaks can also exist as the SPP wave packet is nonmonochromatic [i.e., the line-shape function $p_q^{Q_s} \neq \delta(q - Q_s)$]. With scattering, these peaks can be shifted and broadened, indicating the shifting and broadening of the corresponding resonant pairs. Small side peaks may also be smeared out by the broadening. Note that with the scattering, the polarizations from the numerical results can have more complex behaviors. The peaks in the polarization can also be distorted by the scattering, which has been omitted in the analytic solution.

We first concentrate on the typical case with $R = 34$ nm and $T = 150$ K corresponding to the strong Landau damping regime. The magnitudes of the normalized electron polarization $|P(nk,n'k')/(\delta f\ \bar{B}_s)|$ from the computation are plotted in Fig. 10(a). In the figure, polarizations with different scatterings are plotted by curves with different colors. The contour plots of the polarizations are also shown in the K-q plane, which are useful for identifying the shape and position of the polarizations. The population differences $\delta f = f_{n'}(k') - f_n(k)$ for the resonant pairs are also plotted with orange curves for comparison, with the corresponding contour map plotted in the K-q plane. The polarizations with different scatterings and the population difference have been offset along the q axis for clarification. The corresponding unnormalized electron polarizations $|P(nk,n'k')/\bar{B}_s|$ are also plotted in the similar way in Fig. 10(b) for comparison. Note that all the polarizations are taken at time $t = 2.86$ ps. Polarizations taken at other time show similar behaviors.

In Fig. 10(a), the polarization is plotted for the resonant pair (i) which is the only relevant resonant pair for the damping. The resonant pair is centralized around the resonance corresponding to the SPP central wave vector Q_s, which is represented by the skyblue dots in Fig. 10(a). One finds that without scattering, the corresponding polarization (red curve) exhibits a sharp main peak around the resonance. Several side peaks exist around the main peak. These features agree with the previous discussion. Note that the main peak lies in the regime with large δf, indicating that the SPP absorption by the polarization is strong. Also note that due to the strong resonance, the profile of the unnormalized polarization is mainly decided by the resonance and shares a similar structure as the normalized one.

In the presence of the ei scattering, the polarization is slightly modified. Some side peaks are smeared out. However, the broadening is rather small and the main peak is almost unchanged. This can be better seen by comparing the polarization with the ei scattering (olive curve) to the one without scattering (red curve). According to the previous discussion,

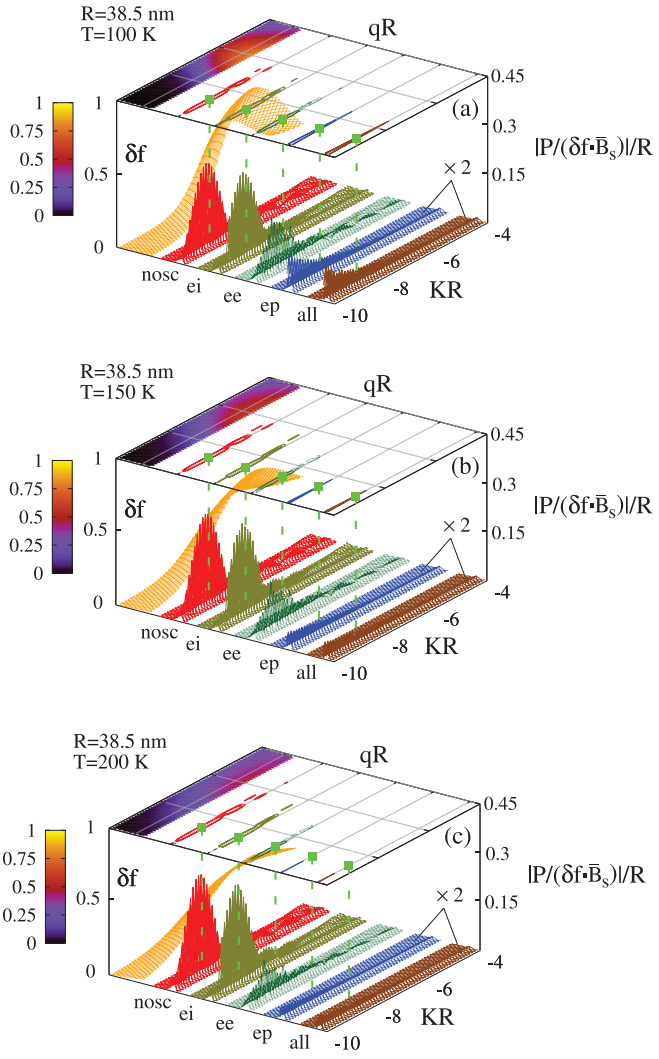

FIG. 11. (Color online) 3D plot and the corresponding contour plot of the normalized electron polarization corresponding to the resonant pair (ii) for (a) $R = 38.5$ nm, $T = 100$ K, (b) $R = 38.5$ nm, $T = 150$ K, and (c) $R = 38.5$ nm, $T = 200$ K. The corresponding population difference is also plotted in the figure. The resonance corresponding to the SPP central wave vector Q_s is shown with green square in the contour plot.

these features indicate that the ei scattering introduces a small broadening.

In the presence of the ee scattering, a shifting of the peaks can be seen clearly by comparing the contour plot of the corresponding polarization (green curve) to the one without scattering (red curve). Note that small side peaks can also be identified with the ee scattering. These features indicate that the ee scattering introduces a large shifting to the corresponding resonant pairs. The broadening due to the ee scattering is small since the small side peaks are not smeared out. It is also noted that the ee scattering can distort the polarization. The peak becomes fragmented and the profile becomes non-Lorentzian. However, as the influence to the SPP damping comes from the summation of the polarizations as indicated by Eq. (12), the effect of these distortion on the SPP damping is marginal.

In the presence of the ep scattering, the peak in the polarization (blue curve) is markedly broadened and all the side peaks are smeared out, indicating that the effect of the ep scattering introduces a large broadening. Note that the maximum of the broadened peak is also shifted compared to the one without scattering. This shows that the ep scattering can also have contribution to the shifting of the resonant pairs. However, due to the large broadening, the effect of such shifting on the SPP damping is marginal. We also point out that due to the large broadening, the profile of the unnormalized polarization is mainly determined by the population difference rather than the resonance, which can be seen from the corresponding unnormalized polarization (blue curve) in Fig. 10(b).

In the presence of all the three scatterings, one finds that the polarization (brown curve) has almost the same profile as the one with the ep scattering only. The broadening and shifting due to the ei and ee scatterings are negligible due to the large broadening introduced by the ep scattering. This indicates that the ep scattering plays the dominant role.

For the weak Landau damping regime, as the scattering has different influence on the SPP damping rate in different temperature regimes. We plot the normalized polarizations in Fig. 11 for three typical cases: (a) $R = 38.5$ nm, $T = 100$ K, (b) $R = 38.5$ nm, $T = 150$ K and (c) $R = 38.5$ nm, $T = 200$ K, corresponding to the low, intermediate, and high temperature regimes, respectively. The polarizations are plotted for the resonant pair (ii) which dominates the SPP damping in these cases. Similar broadening and shifting can also be identified in the figure. Note that in these cases, the shifting due to the ee scattering is rather small and difficult to be identified in the figures.

*yin80@ustc.edu.cn
†mwwu@ustc.edu.cn

[1]R. H. Ritchie, Phys. Rev. **106**, 874 (1957).
[2]C. J. Powell and J. B. Swan, Phys. Rev. **118**, 640 (1960).
[3]C. K. Chen, A. R. B. de Castro, and Y. R. Shen, Phys. Rev. Lett. **46**, 145 (1981).
[4]A. Wokaun, J. P. Gordon, and P. F. Liao, Phys. Rev. Lett. **48**, 957 (1982).
[5]B. Rothenhäusler and W. Knoll, Nature (London) **332**, 615 (1988).
[6]U. Kreibig and M. Vollmer, *Optical Properties of Metal Clusters* (Springer-Verlag, Berlin, 1995).
[7]A. V. Zayats, I. I. Smolyaninov, and A. A. Maradudin, Phys. Rep. **408**, 131 (2005).
[8]J. M. Pitarke, V. M. Silkin, E. V. Chulkov, and P. M. Echenique, Rep. Prog. Phys. **70**, 1 (2007).
[9]F. J. Garcia-Vidal, L. Martin-Moreno, T. W. Ebbesen, and L. Kuipers, Rev. Mod. Phys. **82**, 729 (2010).
[10]H. Raether, *Surface Plasmons* (Springer, Berlin and New York, 1988).
[11]W. L. Barnes, A. Dereux, and T. W. Ebbesen, Nature (London) **424**, 824 (2003).
[12]B. Hecht, H. Bielefeldt, L. Novotny, Y. Inouye, and D. W. Pohl, Phys. Rev. Lett. **77**, 1889 (1996).

[13]K. Kneipp, Y. Wang, H. Kneipp, L. T. Perelman, I. Itzkan, R. R. Dasari, and M. S. Feld, Phys. Rev. Lett. **78**, 1667 (1997).
[14]S. M. Nie and S. R. Emery, Science **275**, 1102 (1997).
[15]H. X. Xu, E. J. Bjerneld, M. Kall, and L. Börjesson, Phys. Rev. Lett. **83**, 4357 (1999).
[16]J. B. Pendry, L. Martin-Moreno, and F. J. Garcia-Vidal, Science **305**, 847 (2004).
[17]E. Ozbay, Science **311**, 189 (2006).
[18]M. Sandtke and L. Kuipers, Nat. Photon. **1**, 573 (2007).
[19]S. A. Maier, *Plasmonics: Fundamentals and Applications* (Springer, New York, 2007).
[20]S. Zhang, D. A. Genov, Y. Wang, M. Liu, and X. Zhang, Phys. Rev. Lett. **101**, 047401 (2008).
[21]J. Homola, S. S. Yee, and G. Gauglitz, Sensors Actuat. B **54**, 3 (1999).
[22]H. A. Atwater and A. Polman, Nat. Mater. **9**, 205 (2010).
[23]D. E. Chang, A. S. Sørensen, P. R. Hemmer, and M. D. Lukin, Phys. Rev. Lett. **97**, 053002 (2006).
[24]A. V. Akimov, A. Mukherjee, C. L. Yu, D. E. Chang, A. S. Zibrov, P. R. Hemmer, H. Park, and M. D. Lukin, Nature (London) **450**, 402 (2007).
[25]R. Kolesov, B. Grotz, G. Balasubramanian, R. J. Stohr, A. A. L. Nicolet, P. R. Hemmer, F. Jelezko, and J. Wrachtrup, Nat. Phys. **5**, 470 (2009).
[26]A. V. Zayats, J. Elliott, I. I. Smolyaninov, and C. C. Davis, Appl. Phys. Lett. **86**, 151114 (2005).
[27]I. I. Smolyaninov, J. Elliott, A. V. Zayats, and C. C. Davis, Phys. Rev. Lett. **94**, 057401 (2005).
[28]J. Takahara, S. Yamagishi, H. Taki, A. Morimoto, and T. Kobayashi, Opt. Lett. **22**, 475 (1997).
[29]Q. Cao and J. Jahns, Opt. Express **13**, 511 (2005).
[30]A. Archambault, F. Marquier, J. J. Greffet, and C. Arnold, Phys. Rev. B **82**, 035411 (2010).
[31]D. J. Bergman and M. I. Stockman, Phys. Rev. Lett. **90**, 027402 (2003).
[32]A. Boltasseva and H. A. Atwater, Science **331**, 290 (2011).
[33]J. A. Schuller, E. S. Barnard, W. Cai, Y. C. Jun, J. S. White, and M. L. Brongersma, Nat. Mater. **9**, 193 (2010).
[34]A. V. Krasavin and N. I. Zheludev, Appl. Phys. Lett. **84**, 1416 (2004).
[35]T. Nikolajsen, K. Leosson, and S. I. Bozhevolnyi, Appl. Phys. Lett. **85**, 5833 (2004).
[36]K. F. MacDonald, Z. L. Sámson, M. I. Stockman, and N. I. Zheludev, Nat. Photon. **3**, 55 (2009).
[37]P. J. Feibelman, Prog. Surf. Sci. **12**, 287 (1982).
[38]W. Ekardt, Phys. Rev. B **31**, 6360 (1985).
[39]A. Liebsch, Phys. Rev. B **36**, 7378 (1987).
[40]K. D. Tsuei, E. W. Plummer, and P. J. Feibelman, Phys. Rev. Lett. **63**, 2256 (1989); K. D. Tsuei, E. W. Plummer, A. Liebsch, E. Pehlke, K. Kempa, and P. Bakshi, Surf. Sci. **247**, 302 (1991).
[41]P. T. Sprunger, G. M. Watson, and E. W. Plummer, Surf. Sci. **269**, 551 (1992).
[42]E. Zaremba and B. N. J. Persson, Phys. Rev. B **35**, 596 (1987).
[43]R. A. Molina, D. Weinmann, and R. A. Jalabert, Phys. Rev. B **65**, 155427 (2002).
[44]G. Weick, R. A. Molina, D. Weinmann, and R. A. Jalabert, Phys. Rev. B **72**, 115410 (2005).
[45]Y. Gao, Z. Yuan, and S. Gao, J. Chem. Phys. **134**, 134702 (2011).
[46]V. M. Silkin, E. V. Chulkov, and P. M. Echenique, Phys. Rev. Lett. **93**, 176801 (2004).
[47]V. M. Silkin and E. V. Chulkov, Vacuum **81**, 186 (2006).
[48]A. J. Hoffman, L. Alekseyev, S. S. Howard, K. J. Franz, D. Wasserman, V. A. Podolskiy, E. E. Narimanov, D. L. Sivco, and C. Gmachl, Nat. Mater. **6**, 946 (2007).
[49]T. Taubner, D. Korobkin, Y. Urzhumov, G. Shvets, and R. Hillenbrand, Science **313**, 1595 (2006).
[50]J. M. Luther, P. K. Jain, T. Ewers, and A. P. Alivisatos, Nat. Mater. **10**, 361 (2011).
[51]D. V. Seletskiy, M. P. Hasselbeck, J. G. Cederberg, A. Katzenmeyer, M. E. Toimil-Molares, F. Léonard, A. A. Talin, and M. Sheik-Bahae, Phys. Rev. B **84**, 115421 (2011).
[52]M. S. Vitiello, D. Coquillat, L. Viti, D. Ercolani, F. Teppe, A. Pitanti, F. Beltram, L. Sorba, W. Knap, and A. Tredicucci, Nano Lett. **12**, 96 (2011).
[53]J. Gómez Rivas, J. A. Sánchez-Gil, M. Kuttge, P. Haring Bolivar, and H. Kurz, Phys. Rev. B **74**, 245324 (2006).
[54]J. Gómez Rivas, M. Kuttge, H. Kurz, P. H. Bolivar, and J. A. Sánchez-Gil, Appl. Phys. Lett. **88**, 082106 (2006).
[55]T. H. Isaac, W. L. Barnes, and E. Hendry, Appl. Phys. Lett. **93**, 241115 (2008).
[56]G. V. Naik and A. Boltasseva, Phys. Stat. Sol. (RRL) **4**, 295 (2010).
[57]M. Galli, D. Gerace, A. Politi, M. Liscidini, M. Patrini, L. C. Andreani, A. Canino, M. Miritello, R. L. Savio, A. Irrera, and F. Priolo, Appl. Phys. Lett. **89**, 241114 (2006).
[58]L. Tang, S. E. Kocabas, S. Latif, A. K. Okyay, D.-S. Ly-Gagnon, K. C. Saraswat, and D. A. B. Miller, Nat. Photon. **2**, 226 (2008).
[59]R. J. Walters, R. V. A. van Loon, I. Brunets, J. Schmitz, and A. Polman, Nat. Mater. **9**, 21 (2010).
[60]M. P. Hasselbeck, D. Seletskiy, L. R. Dawson, and M. Sheik-Bahae, Phys. Status Solidi C **5**, 253 (2008).
[61]For semiconductors, the scattering between the SPP and the LO phonons can also lead to the SPP damping [G. C. Cho, T. Dekorsy, H. J. Bakker, R. Hovel, and H. Kurz, Phys. Rev. Lett. **77**, 4062 (1996)], which plays the dominant role for the SPP with small wave vectors (see Ref. 51).
[62]D. H. Ehlers and D. L. Mills, Phys. Rev. B **34**, 3939 (1986); **36**, 1051 (1987).
[63]G. R. Bell, C. F. McConville, and T. S. Jones, Phys. Rev. B **54**, 2654 (1996).
[64]G. R. Bell, T. D. Veal, J. A. Frost, and C. F. McConville, Phys. Rev. B **73**, 153302 (2006).
[65]F. J. García de Abajo, Rev. Mod. Phys. **82**, 209 (2010).
[66]H. Haug and A.-P. Jauho, *Quantum Kinetics in Transport and Optics of Semiconductors* (Springer-Verlag, Berlin, 1996).
[67]M. W. Wu, J. H. Jiang, and M. Q. Weng, Phys. Rep. **493**, 61 (2010).
[68]A. Konar and D. Jena, J. Appl. Phys. **102**, 123705 (2007).
[69]N. G. Hörmann, I. Zardo, S. Hertenberger, S. Funk, S. Bolte, M. Döblinger, G. Koblmüller, and G. Abstreiter, Phys. Rev. B **84**, 155301 (2011); M. Möller, M. M. de Lima, A. Cantarero, L. C. O. Dacal, J. R. Madureira, F. Iikawa, T. Chiaramonte, and M. A. Cotta, *ibid.* **84**, 085318 (2011).
[70]R. Loudon, *The Quantum Theory of Light*, 3rd ed. (Oxford University Press, Oxford, 2000).
[71]H. Ditlbacher, A. Hohenau, D. Wagner, U. Kreibig, M. Rogers, F. Hofer, F. R. Aussenegg, and J. R. Krenn, Phys. Rev. Lett. **95**, 257403 (2005).
[72]H. T. Miyazaki and Y. Kurokawa, Phys. Rev. Lett. **96**, 097401 (2006).

[73]L. Cao, R. A. Nome, J. M. Montgomery, S. K. Gray, and N. F. Scherer, Nano Lett. **10**, 3389 (2010).
[74]S. A. Dayeh, D. P. R. Aplin, X. Zhou, P. K. L. Yu, E. T. Yu, and D. Wang, Small **3**, 326 (2007).
[75]For sufficiently long SPP wave packet ($L \gtrsim 100R$), the results are not sensitive to the wave packet length L.
[76]K. P. Charlé, W. Schulze, and B. Winter, Z. Phys. D **12**, 471 (1989).
[77]C. Brećhignac, Ph. Cahuzac, J. Leygnier, and A. Sarfati, Phys. Rev. Lett. **70**, 2036 (1993).
[78]S. Mochizuki, M. Sasaki, and R. Ruppin, J. Phys.: Condens. Matter **9**, 5801 (1997).
[79]The influence of the ei scattering depends on both the impurity configuration and the impurity density. In addition to the surface impurities, we have also performed the calculation for bulk-like impurities (i.e., impurities evenly distributed inside the nanowire. The corresponding line density of the bulk impurities is set equal to the line density of the surface impurities n_i). For both impurity configurations, we have checked that the influence of the ei scattering remains very small for $n_i < 5n_e$.
[80]A. Bergara, J. M. Pitarke, and R. H. Ritchie, Phys. Rev. B **60**, 16176 (1999).
[81]R. H. Ritchie and R. E. Wilems, Phys. Rev. **178**, 372 (1969).
[82]G. Barton, Rep. Prog. Phys. **42**, 963 (1979).
[83]I. Villó-Pérez and N. R. Arista, Surf. Sci. **603**, 1 (2009).
[84]E. Prodan, C. Radloff, N. Halas, and P. Nordlander, Science **302**, 419 (2003); E. Prodan and P. Nordlander, J. Chem. Phys. **120**, 5444 (2004).
[85]A. F. Slachmuylders, B. Partoens, W. Magnus, and F. M. Peeters, Phys. Rev. B **74**, 235321 (2006).
[86]C. Ell and H. Haug, Phys. Status Solidi B **159**, 117 (1990).
[87]D. B. Tran Thoai and H. T. Cao, Solid State Commun. **111**, 67 (1999).
[88]S. N. Klimin, E. P. Pokatilov, and V. M. Fomin, Phys. Status Solidi B **184**, 373 (1994).
[89]C. R. Bennett, N. C. Constantinou, M. Babiker, and B. K. Ridley, J. Phys.: Condens. Matter **7**, 9819 (1995).
[90]A. L. Vartanian, Phys. Status Solidi B **242**, 1482 (2005).